Combined high-resolution seismostratigraphic and morphobathymetric analysis reveals glacial history of the northwestern Chukchi margin, Arctic Ocean

Sookwan Kim[1*], Leonid Polyak[2], Young Jin Joe[1,3], Frank Niessen[4], Hyoung Jun Kim[1], Yeonjin Choi[1,5], Seung-Goo Kang[1], Jong Kuk Hong[1], Seung-Il Nam[1], and Young Keun Jin[1*]

[1]Korea Polar Research Institute, Incheon, 21990, Republic of Korea

[2]Byrd Polar and Climate Research Center, The Ohio State University, 1090 Carmack Road, Columbus, OH, 43210, USA

[3]Department of Earth and Marine Sciences, Jeju National University, Jeju, 63243, Republic of Korea

[4]Alfred Wegener Institute (AWI), Helmholtz Centre for Polar and Marine Research, D-27568, Bremerhaven, Germany

[5]Korea Maritime and Ocean University, Busan, 49112, Republic of Korea

*Corresponding authors: S. Kim (skwan@kopri.re.kr) and Y. K. Jin (ykjin@kopri.re.kr)

Key Points:

- Detailed sub-bottom profiler and multibeam echosounder data were acquired at the northwestern Chukchi margin.
- The new geophysical data grid reveals a three-dimensional geometry and distribution of glaciogenic sediments and geomorphic features.
- Seafloor mapping results indicate four major glacial events with variable grounded ice extent and flow direction.

Abstract

High-resolution seafloor mapping provides insights into the dynamics of past ice-sheets/ice-shelves on high-latitude continental margins. Geological/geophysical studies in the Arctic Ocean suggest widespread Pleistocene ice grounding on the Chukchi–East Siberian continental margin. However, flow directions, timing, and behavior of these ice masses are not yet clear due to insufficient data. We present a combined seismostratigraphic and morphobathymetric analysis of the Chukchi Rise off the northwestern Chukchi margin using the densely acquired sub-bottom profiler (SBP) and multibeam echosounder (MBES) data. Comparison with deeper airgun seismic records shows that the SBP data cover most of the glaciogenic stratigraphy possibly spanning ca. 0.5–1 Ma. Based on the stratigraphic distribution and geometry of acoustically transparent glaciogenic diamictons, the lateral and vertical extent of southern-sourced grounded ice became smaller over time. The older deposits are abundant as debris lobes on the slope contributing to a large trough mouth fan, whereas younger till wedges are found at shallower depths. MBES data show two sets of mega-scale lineations indicating at least two fast ice-streaming events of different ages. Contour-parallel recessional morainic ridges mark a stepwise retreat of the grounded ice margin, likely controlled by rising sea levels during deglaciation(s). The different inferred directions of ice advances and retreats reflect complex geomorphic settings on the borderland. The overall picture shows that the Chukchi Rise was an area of intense interaction(s) of different ice-sheets/ice-shelves. In addition to glaciogenic deposits, we identify a number of related or preceding seabed features including mounds, gullies/channels, and sediment waves.

1 Introduction

Understanding the dynamics of marine-based ice sheets is a critical prerequisite for predicting the responses of modern glacial systems to the warming climate and rising sea levels (e.g., DeConto & Pollard, 2016; Howat et al., 2007). This task requires thorough geological and geophysical investigation of high-latitude continental margins and adjacent borderlands for understanding the build-up and decay mechanisms of the past ice sheets (Dowdeswell et al., 2016 and references therein). While comprehensive data have been collected from the Polar North Atlantic margins since the late 20th century (Elverhøi et al., 1998), the Quaternary glacial history of the Arctic Ocean remained largely speculative until the last two decades. Recent marine geophysical data employing high-resolution seafloor mapping technologies indicate the extensive impact of grounded ice-sheets/ice-shelves on the continental margins, as well as bathymetric highs in the central Arctic Ocean (Dove et al., 2014; Jakobsson, 1999; Jakobsson et al., 2008, 2014, 2016; Niessen et al., 2013; Polyak et al., 2001). In particular, a wealth of new data has been collected from the Chukchi–East Siberian margin and the adjacent borderland in the western Arctic Ocean since the late 2000s due to the rapid retreat of sea-ice cover (Coakley et al., 2011; Darby et al., 2005; Jokat, 2009; SWERUS Scientific Party, 2016). The acquired data demonstrate a complex pattern of grounded-ice impact on the seafloor interpreted as recurring glacial flows from the Laurentide, East Siberian, and Chukchi ice centers (Dove et al., 2014; Jakobsson et al., 2005, 2008, 2014; Niessen et al., 2013; Polyak et al., 2007). This picture indicates a critical role of this region for understanding the overall Arctic glacial history, while the timing, extent, and provenance of glacial events remain poorly known.

In this paper, we focus on the western side of the Chukchi Rise, a geological structure extending north from the Chukchi continental shelf (Figure 1). The Chukchi Rise and adjacent seafloor structures were shown to have multiple glaciogenic bedforms indicative of glacial flows potentially originating from the Laurentide, East Siberian, and Chukchi ice-spreading centers (Dove et al., 2014; Jakobsson et al., 2008, 2014; Polyak et al., 2001, 2007) (Figure 1a). The western Chukchi Rise facing the East Siberian margin is a key but poorly constrained area for understanding these glacial interactions. We analyze new, detailed seismostratigraphic and geomorphic data from this area for empirical constraints on past ice-sheet dynamics and related sedimentary processes. Our analysis is based on the combined high-resolution sub-bottom profiler (SBP) and multibeam echosounder (MBES) data revealing previously unexplored sedimentary structures, stratigraphy, and submarine landforms. These densely collected geophysical data (Figure 1b) allow for tracing the three-dimensional geometry of individual seafloor and subsurface formations, which provide clues for spatio-temporal distribution of the depositional/erosional glaciogenic features and related seabed forming processes (Dowdeswell et al., 2004, 2016; C. H. Eyles & Eyles, 2010; Rebesco et al., 2016). This empirical evidence augments sediment-core stratigraphy from neighboring areas (Joe et al., 2020; Polyak et al., 2007; Schreck et al., 2018) and ice sheet modeling studies (Colleoni et al., 2016; Gasson et al., 2018), and thus sheds new light on the glacial history of the Chukchi–East Siberian continental margin. The generated data also provide valuable context for potential scientific drilling projects in the western Arctic Ocean.

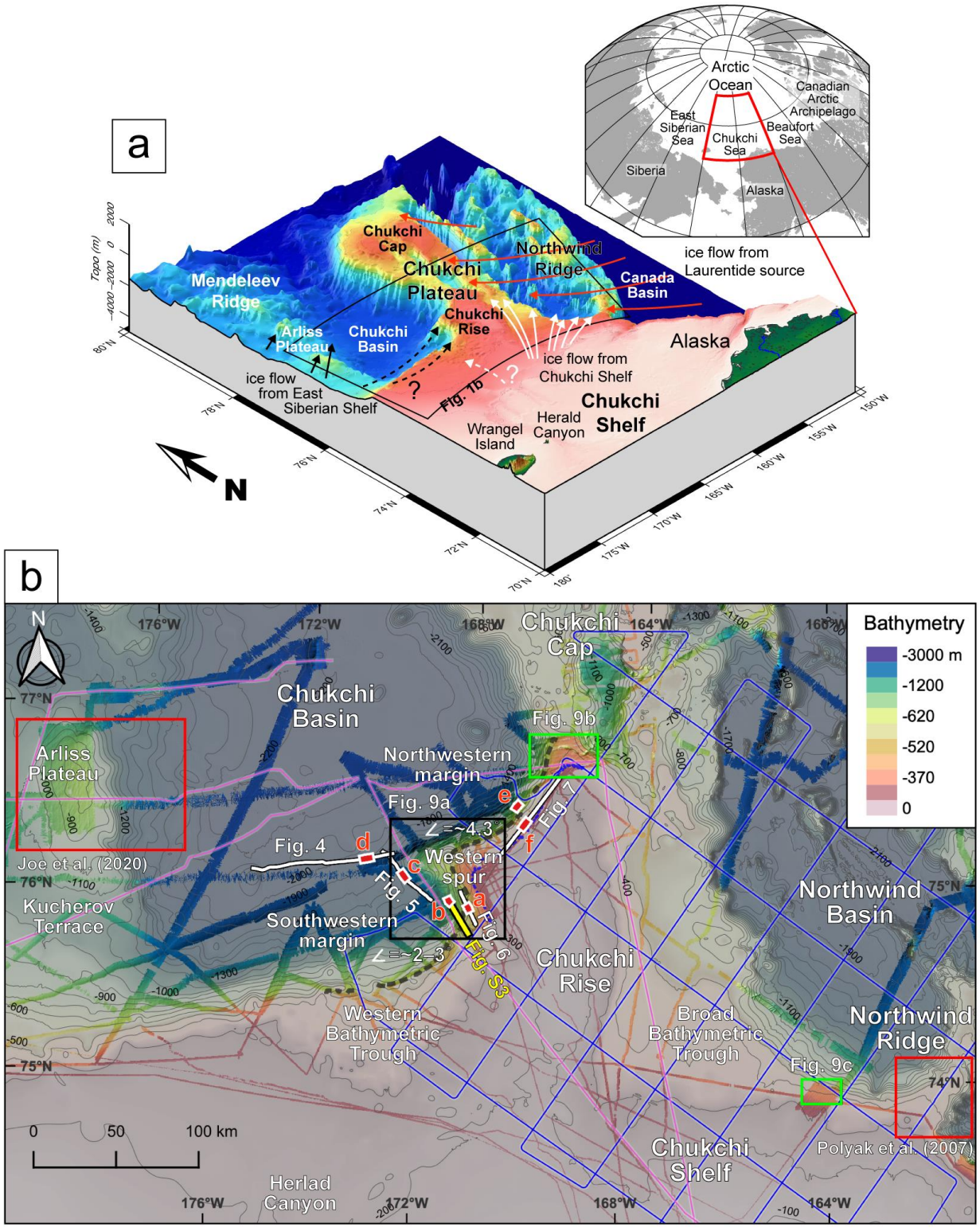

Figure 1. **(a)** Location map of the Chukchi Borderland in the Arctic Ocean (upper right inset) and a bathymetric map of the Chukchi Borderland (IBCAO version 4.0; Jakobsson et al., 2020). Color-coded arrows indicate ice flow directions inferred in prior studies (Dove et al., 2014;

Jakobsson et al., 2008, 2014; Niessen et al., 2013; Polyak et al., 2001); from the East Siberian (black), Chukchi margin (white), and Laurentide source (red); dashed arrows indicate more tentative interpretations. A black fan-shaped rectangle outlines the study area shown in panel 1b. **(b)** Data location map of the western side of the Chukchi Rise subdivided into the northwestern and southwestern margins and the western spur. Multibeam bathymetry data collected by the IBRV *Araon* (bright-colored) is overlaid on the regional bathymetry (dim-colored) with 100-m contour intervals. Thick white lines are the key SBP data shown in Figures 4 to 7. Labeled thick red segments are locations of the SBP data columns ***a***–***f*** in Figure 2. The black rectangle outlines the detailed survey area shown in Figures 9a and S5. Other rectangles show the location of additional ARA03B data (green, Figures 9b and 9c) and the study areas from Polyak et al. (2007) on the Northwind Ridge and Joe et al. (2020) on the Arliss Plateau (red). White numbers show the upper slope gradients. Blue and purple lines are regional geophysical data grids of MGL1112 (Coakley et al., 2011; Dove et al., 2014) and ARK-XXIII/3 (Hegewald & Jokat, 2013; Jokat, 2009), respectively. A thick yellow line crossing the outer shelf to the upper-mid slope is a multichannel seismic profile along the trough mouth fan at the southwestern margin (Figure S3). Dark gray and blue dashed lines are 600-mwd and 350-mwd isolines marking the shelf edge and the limit of iceberg plowmarks, respectively.

2 Background

The Chukchi Borderland in the western Arctic Ocean is comprised of the north–south trending bathymetric highs and troughs (Hall, 1990) (Figure 1a). The Chukchi Rise is an immediate extension of the Chukchi Shelf separated by a saddle-like depression from the Chukchi Cap to the north (Hegewald & Jokat, 2013; Shaver & Hunkins, 1964). The Chukchi Basin to the west and the Northwind Basin to the east separate the Chukchi Rise from the East Siberian margin and the Northwind Ridge, respectively. The relatively flat top shelf of the Chukchi Rise has ~200 m water depth (mwd) and less than 0.1˚ of slope gradient measured along a ~100 km north-south transect (Jakobsson et al., 2020). The western side of the Chukchi Rise shelf has a generally steeper inclination (ca. 0.5–0.7˚) from the crest to the shelf break at ~500–600 mwd than the eastern side (ca. 0.3˚). The slope gradient from the shelf break to middle slope at ~1000–1100 mwd varies from gentler (ca. 2.6–3.3˚) in the southwestern Chukchi Rise to steeper (ca. 4.6˚) in the northwestern Chukchi Rise (white numbers in Figure 1b). The mid-lower slope gradient (from ~1100 to 2200 mwd) on the southwestern margin is ~0.6˚. A triangular-shaped bathymetric high, named the western spur in this study, protrudes westward from the middle of the Chukchi Rise ~20 km into the Chukchi Basin (Figure 1b). A broad, seaward-dipping (ca. 0.3˚) bathymetric depression (Western Bathymetric Trough) associated with the Herald Canyon on the Chukchi Shelf separates the western slope of the Chukchi Rise from the continental margin (Figure 1b). A similar bathymetric feature on the eastern side of the Chukchi Rise has been named the Broad Bathymetric Trough by Dove et al. (2014). Both troughs are characteristically short and wide (Western Bathymetric Trough ~20–60 km long and 150 km wide) unlike the well-developed cross-shelf troughs on the Arctic continental margins (e.g., Bear Island and M'Clure Strait troughs in Batchelor & Dowdeswell, 2014).

Multiple glaciogenic sediment accumulations and submarine landforms, such as mega-scale glacial lineations (MSGL), moraine ridges, and iceberg plowmarks, were identified by the

recent geophysical surveys on the Chukchi Borderland (Dove et al., 2014; Hegewald & Jokat, 2013; Ilhan & Coakley, 2018; Jakobsson et al., 2005, 2008; Polyak et al., 2001, 2007) and the East Siberian margin (Joe et al., 2020; Niessen et al., 2013). These seafloor features were interpreted to have been formed by grounding of several-hundred-meters thick ice caps and/or ice shelves that impacted the Chukchi–East Siberian margin during several Quaternary glaciations. The grounded ice masses on the Chukchi Borderland may have originated from the Laurentide Ice Sheet to the east, the East Siberian margin to the west, and the Chukchi Shelf to the south, possibly with the local ice-cap/ice-sheet covering the shallowest areas such as the Chukchi Plateau (Dove et al., 2014; Jakobsson et al., 2005, 2008, 2014; Polyak et al., 2001, 2007) (Figure 1a). The deep-penetrating airgun seismic profiles across the shelf edge of the Chukchi–East Siberian continental margin including the Chukchi Rise (purple and blue lines in Figure 1b) show that the marine Neogene deposits on the outer shelf and slope are truncated by glaciogenic sedimentary units downlapping on the pre-glacial strata (Dove et al., 2014; Hegewald & Jokat, 2013; Ilhan & Coakley, 2018; Niessen et al., 2013). These stratigraphic features indicate that large amounts of sediment were eroded by the grounded ice from the shelf and transported to the slope. Based on the stratigraphic position of the resulting regional unconformity within the Plio-Pleistocene deposits, the Chukchi continental margin has a long glacial history (Hegewald & Jokat, 2013), but its timeline, patterns, and mechanisms involved are still poorly understood.

3 Materials and methods

All of the new geophysical data used in this study were acquired by the 2015–2019 IBRV *Araon* Arctic Expeditions ARA06B/06C, ARA07C, ARA09C, and ARA10C. These data fill a coverage gap between regional geophysical data of the prior expeditions MGL1112 (Coakley et al., 2011) and ARK-XXIII-3 (Jokat, 2009) (Figure 1b). For a broader regional coverage, we also utilized the 2012 ARA03B data from the more northern and eastern parts of the Chukchi Rise (Figure 1b). This paper is based primarily on the SBP and MBES data, with some of the airgun seismic records used for verifying the identification of the major stratigraphic boundaries. The frequency range of SBP data was set to 2.5–7.0 kHz with the ping rates of 1–2 s depending on the water depth and recording window length (400–500 ms). These settings provided a sediment penetration of tens of meters to less than 100 m, depending on the seabed morphology and geological conditions, with a vertical resolution of ~0.5 m or better. During the ARA10C SBP/MBES survey, the airgun seismic data were simultaneously collected using two Sercel Generator-Injector (G.I.) guns (each 355 in^3 volume; 250 in^3 for generator and 105 in^3 for injector) and a 1.5-km-long Sercel Sentinel solid-type streamer (120 channels). The MBES system recorded travel times and amplitudes of reflected signals with a wide beam angle (–65˚ to +65˚). The swath width of MBES data is ~4.3 times the water depth. The MBES bathymetry data were frequently calibrated using the sound velocity profiles of the conductivity-temperature-depth (CTD) castings. The MBES backscatter intensities were recorded simultaneously with the bathymetry data acquisition. The quality of all data varied with the weather, sea ice conditions, and ship speed.

The processing procedure applied to the SBP data includes delay-time shifting, resampling, signal enveloping, spherical divergence correction using Seismic Unix. The coordinates of each ping point number (PN) were extracted from the SBP data header. The

airgun seismic data were processed through conventional processing steps, including setup of the geometry, debubble, velocity analysis, multiple attenuation, pre-stack time migration, common mid-point stack, and seafloor muting using Schlumberger Omega 2017. The processed SBP and airgun seismic data were imported into the seismic data interpretation software SeisWare Geophysics for acoustic facies analysis, horizon picking, seismic correlation, and isopach mapping. The sediment depths were estimated from the two-way travel time using 1500 m/s sound speed. The resolved stratigraphic boundaries were traced on the SBP and airgun seismic data (Figures 2 and S1–S3). The identified seismostratigraphic units/subunits were gridded to a resolution of 100 m using a minimum curvature interpolation and were presented in the sediment thickness maps (Figure 3 and S4). The new, high-resolution MBES bathymetry and backscatter data were processed using CARIS HIPS&SIPS. The processed MBES results were gridded to a resolution of 20 m and were superimposed on the regional bathymetry grid (IBCAO V4; Jakobsson et al., 2020) using the QGIS software.

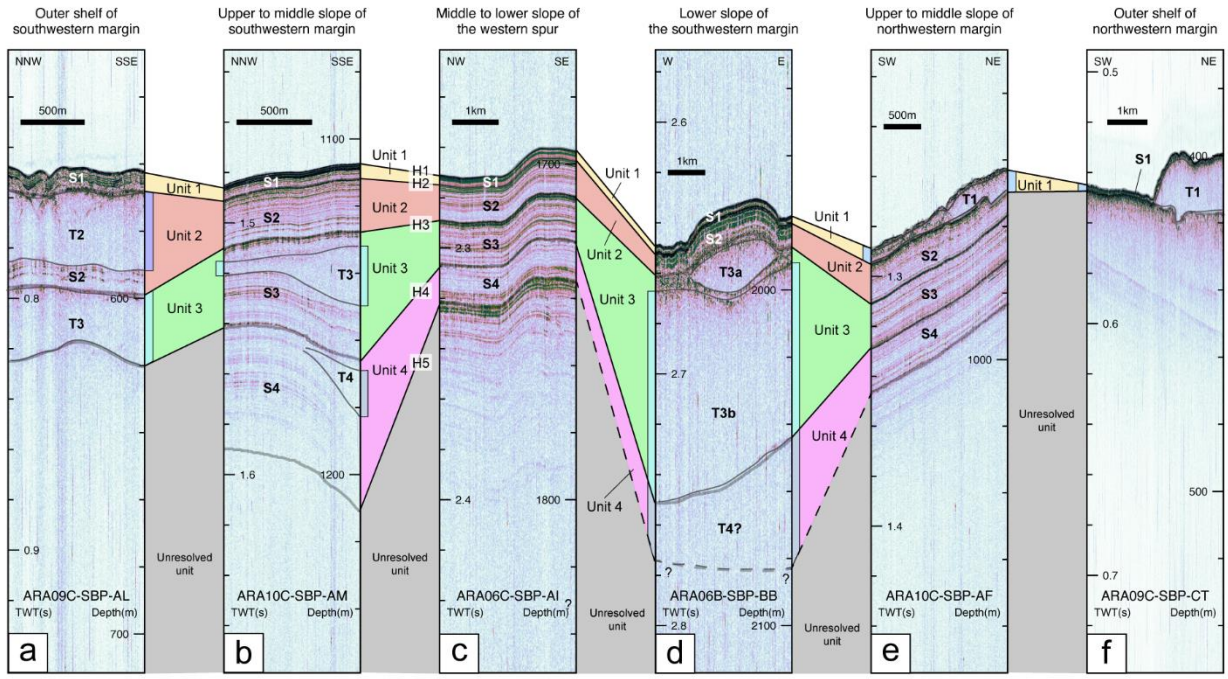

Figure 2. **(a)**–**(f)** The SBP data columns summarizing the seismic stratigraphy of the western Chukchi Rise margin. Seismostratigraphic units U4 to U1 are defined by the laterally continuous reflectors marked by thick gray solid lines. Depositional bodies (lenses) T4 to T1 are the acoustically transparent subunits (facies) within units U4 to U1. The location of the SBP columns ***a***–***f*** is shown in Figure 1b.

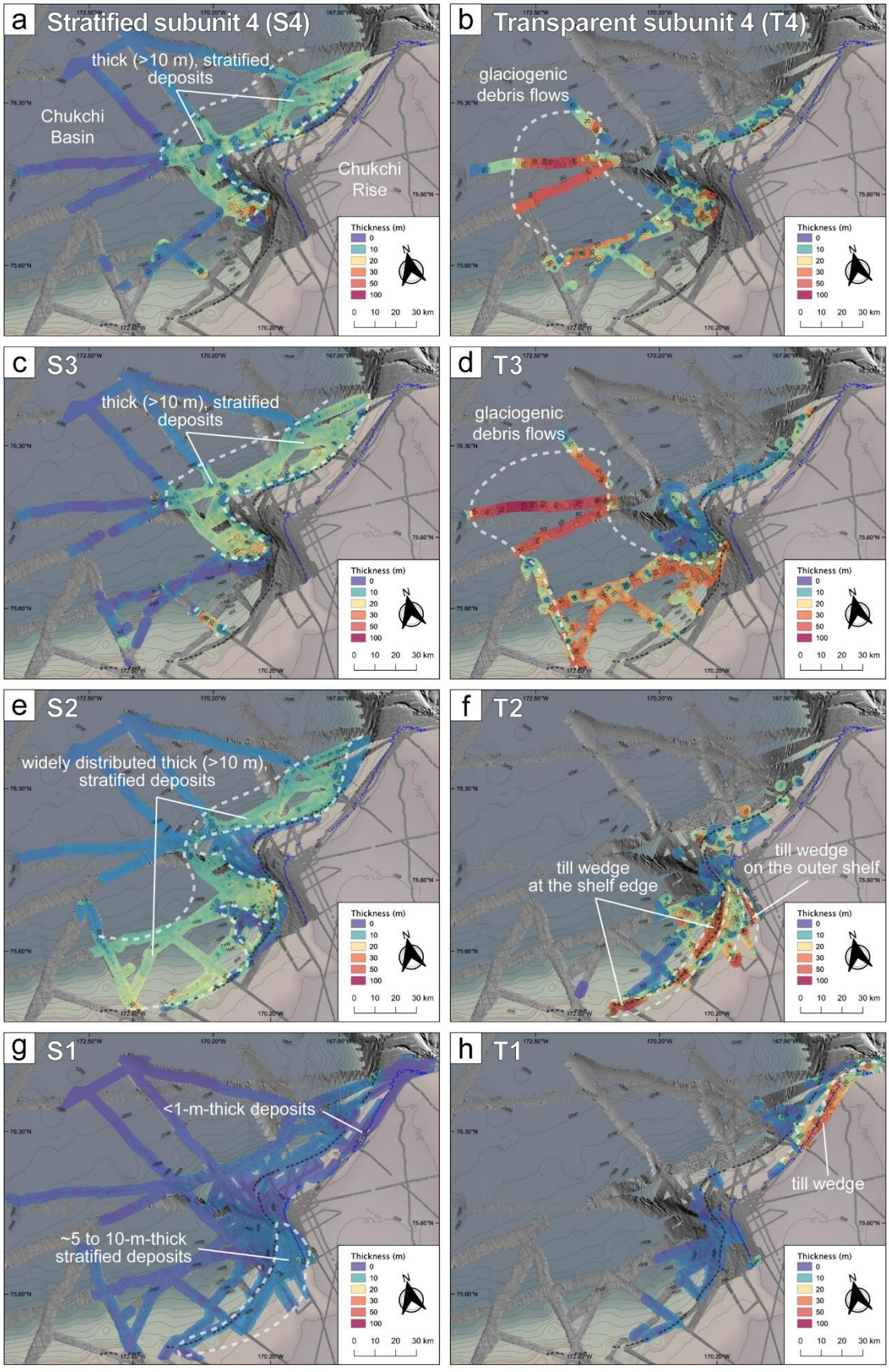
a Stratified subunit 4 (S4)
thick (>10 m), stratified deposits
Chukchi Basin
Chukchi Rise
b Transparent subunit 4 (T4)
glaciogenic debris flows
c S3
thick (>10 m), stratified deposits
d T3
glaciogenic debris flows
e S2
widely distributed thick (>10 m), stratified deposits
f T2
till wedge at the shelf edge
till wedge on the outer shelf
g S1
<1-m-thick deposits
~5 to 10-m-thick stratified deposits
h T1
till wedge
Thickness (m)
0
10
20
30
50
100
0 10 20 30 km

202

Figure 3. Sediment thickness maps of the acoustically stratified subunits S4 to S1 **(a, c, e, g)** and the acoustically transparent subunits T4 to T1 **(b, d, f, h)** on the outer shelf and slope of the western Chukchi Rise. The hillshaded multibeam bathymetry data is shown in gray-tones on the regional bathymetry. The sediment thickness was converted from milliseconds to meters at 1500 m/s sound velocity. The lower boundaries of S4 and T4 on the mid-lower southwestern slope were partially defined in the SBP data (Figure 4), the thickness of S4/T4 is tentatively plotted in Figures 3a and 3b.

4 Results

4.1 Seismostratigraphy

The SBP data show the stratal geometries, internal structures, stacking patterns, and stratigraphic relationships in the uppermost, mostly ~20–40-m-thick deposits. The covered sedimentary succession was divided into four major seismostratigraphic units designated as U4 to U1 from the oldest to the youngest (Figures 2 and S4). The unit boundaries were identified by erosional unconformities and/or otherwise laterally sub-continuous, high-amplitude seismic reflections H1–H5 (where H1 is a seafloor) in both of the SBP and accompanying airgun seismic records (Figures 2 and S1–S3). These reflectors have the best expression at the foot of the western Chukchi Rise slope, from where they were traced up-slope using the key SBP lines (Figure S1). Although the SBP grid in the northwestern area is relatively sparse, a consistent stacking pattern of the identified units and their mostly continuous boundaries enable the seismostratigraphic interpretation for most of the western Chukchi Rise margin (Figures 2, 3, and S1).

Each major unit is composed of two seismostratigraphic facies (subunits). One is acoustically stratified and shows parallel to subparallel internal configuration, high-to-medium lateral continuity, and low-to-medium amplitude reflections (Figure 2). The stratified subunits, S4–S1, mimic a smooth or undulated geometry of the underlying unit boundaries in most of the study area (Figures 2b, 2c, and 2e). The other facies type is distinguished in lens- or sheet-shaped deposits with a transparent/semi-transparent acoustic signature (Figure 2). The lower boundary of the transparent subunits, T4–T1, typically truncates the internal reflections or the underlying units (Figure 2a–2e and 2f). These boundaries correspond to the main reflectors between the units, otherwise the upper and lower boundaries of the transparent subunits pinch out and continue as internal reflections (Figures 2b, 2d, and 2f). The constructed isopach maps show the distribution of sediment thickness of the identified stratified subunits S4 to S1 and transparent subunits T4 to T1 (Figure 3). Below we describe these stratigraphic divisions from bottom to top.

4.1.1 Unresolved strata

The oldest deposits captured by the SBP records are represented by the stratigraphically unresolved strata with subparallel internal reflections. At the mid-lower slope of the southwestern Chukchi Rise, the unresolved strata show a stacking pattern similar to the overlying units U4–U1 (PN 5300–6000 in Figure 4 and PN 3000–6000 in Figure 5). In contrast, on the outer shelf of the western Chukchi Rise, the SBP data show that wavy, subparallel internal reflections of stratigraphically unresolved lower strata are truncated by the base of the major

units and subunits (PN 3500–4500 in Figure 6 and PN 2000–12000 in Figure 7). These records are similar to the wavy, continuous reflections that are overlain by the thick package of glaciogenic sediments along the slope of the Chukchi margin as shown by the prior and ARA10C airgun seismic data (Dove et al., 2014; Hegewald & Jokat, 2013; Ilhan & Coakley, 2018) (Figures 1 and S3).

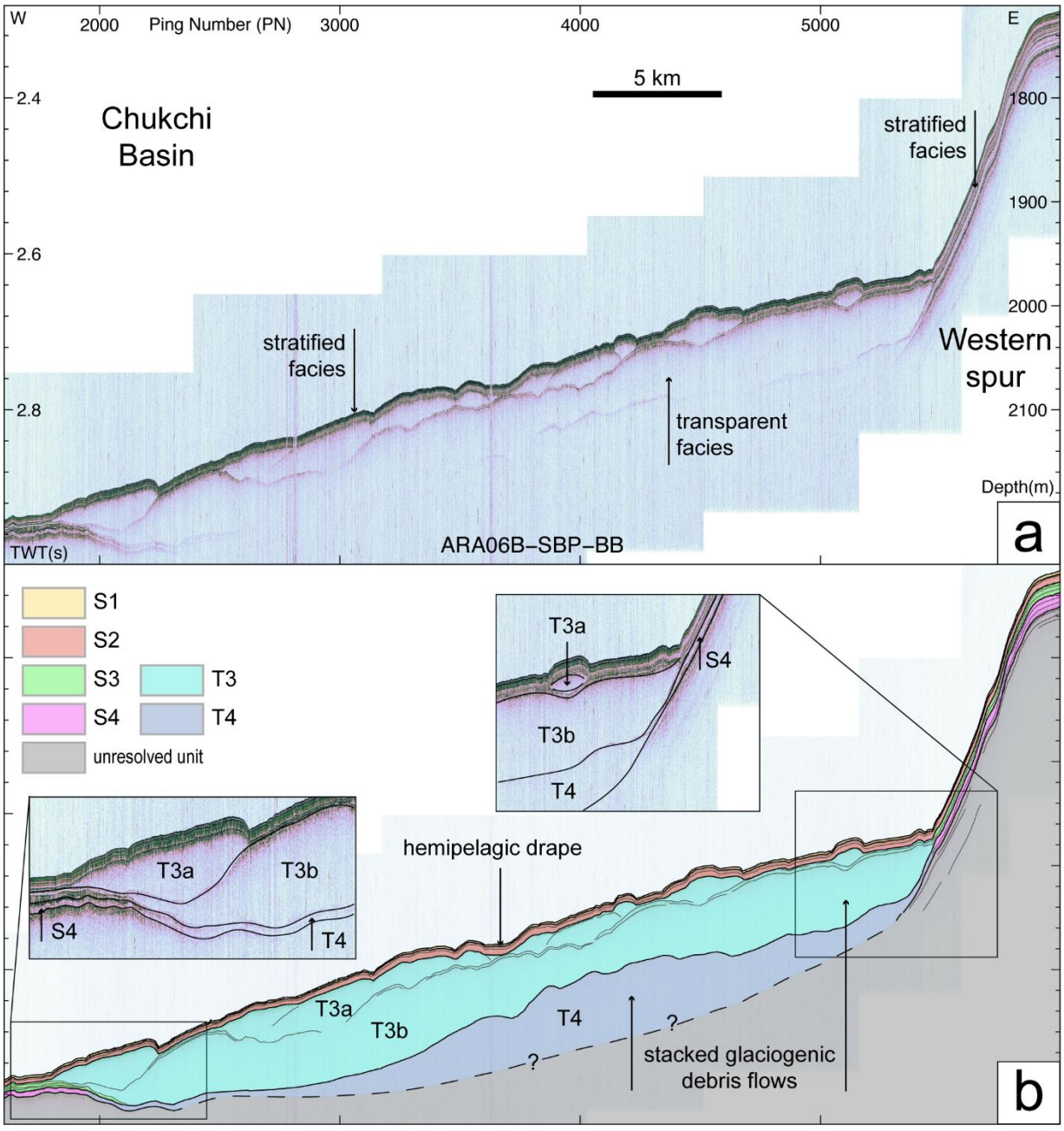

Figure 4. Uninterpreted **(a)** and interpreted **(b)** sub-bottom profile ARA06B-SBP-BB extended into the Chukchi Basin (see Figure 1b for location). The SBP data show stacked glaciogenic

debris lobes of acoustically transparent subunits T4 and T3 interbedded with acoustically stratified subunits S4–S1. Vertical axes are two-way travel time in the left and depth in meter at 1500 m/s sound speed in the right.

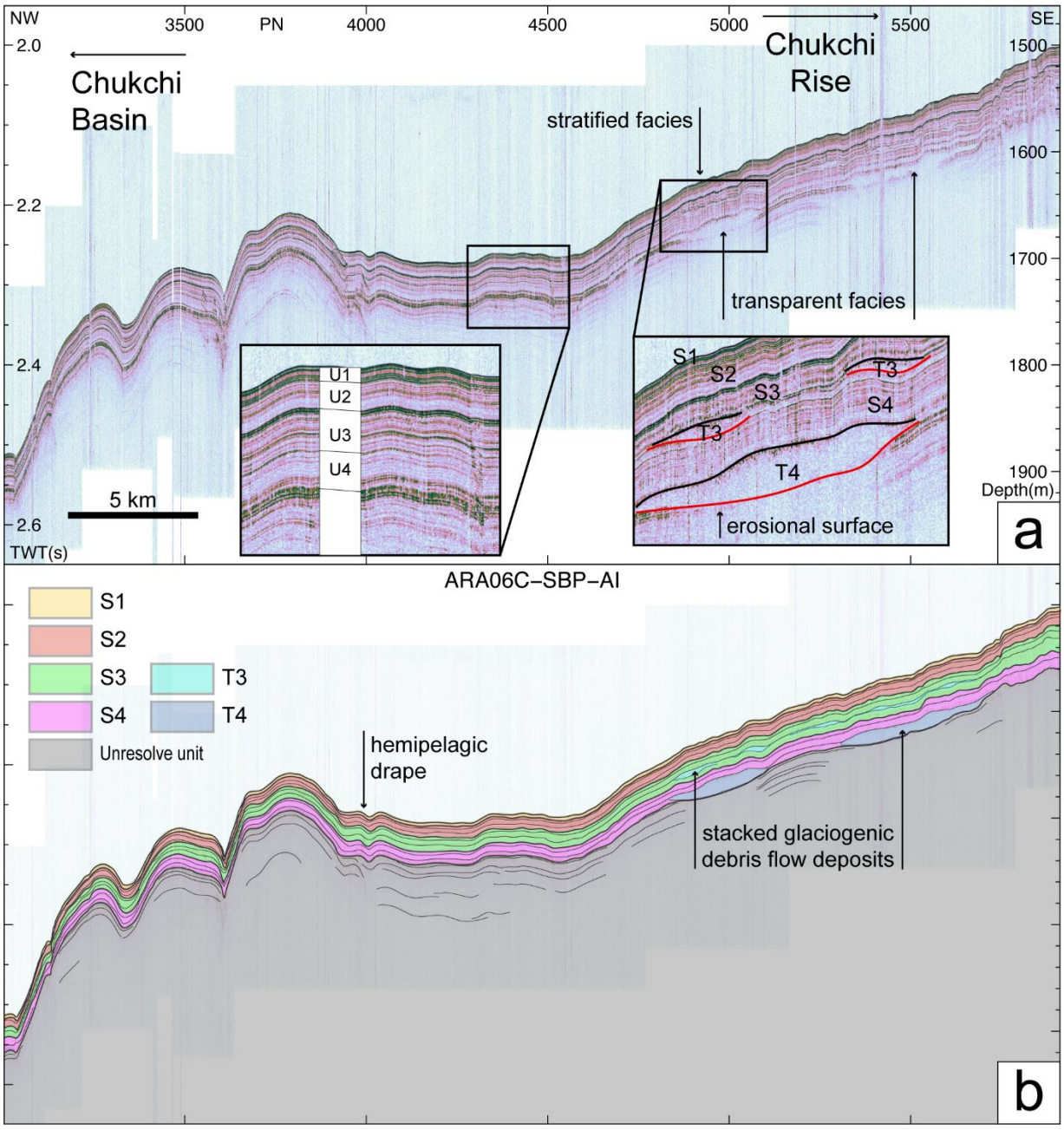

Figure 5. Uninterpreted **(a)** and interpreted **(b)** sub-bottom profile ARA06C-SBP-AI showing acoustically transparent T4 and T3 lenses within acoustically stratified sediments of S4 to S1 on the middle to lower southwestern slope (see Figure 1b for location).

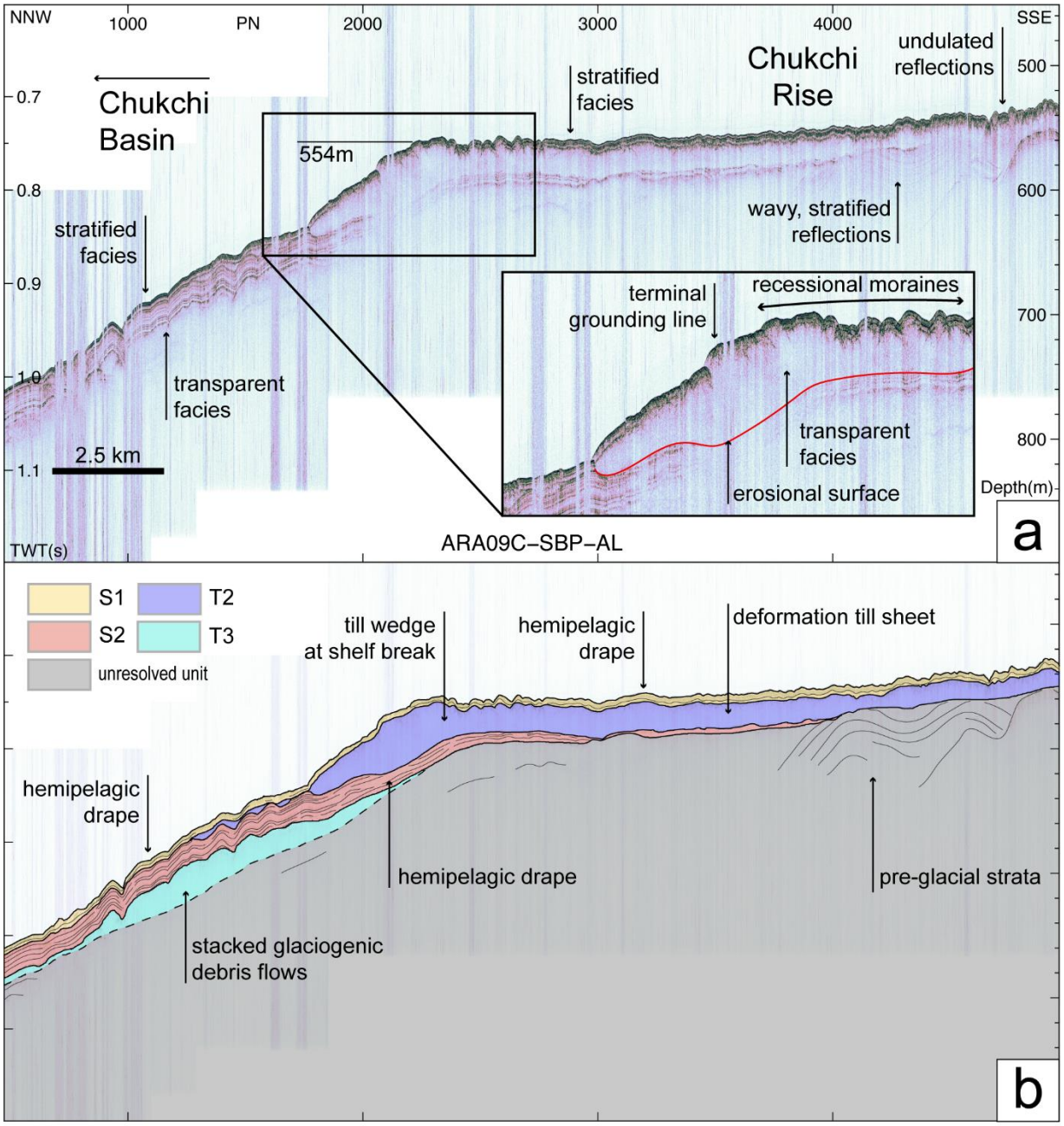

Figure 6. Uninterpreted **(a)** and interpreted **(b)** sub-bottom profile ARA09C-SBP-AL showing acoustically transparent deposits T2 and T3 interbedded with acoustically stratified sediments on the southwestern outer shelf to upper slope (see Figure 1b for location).

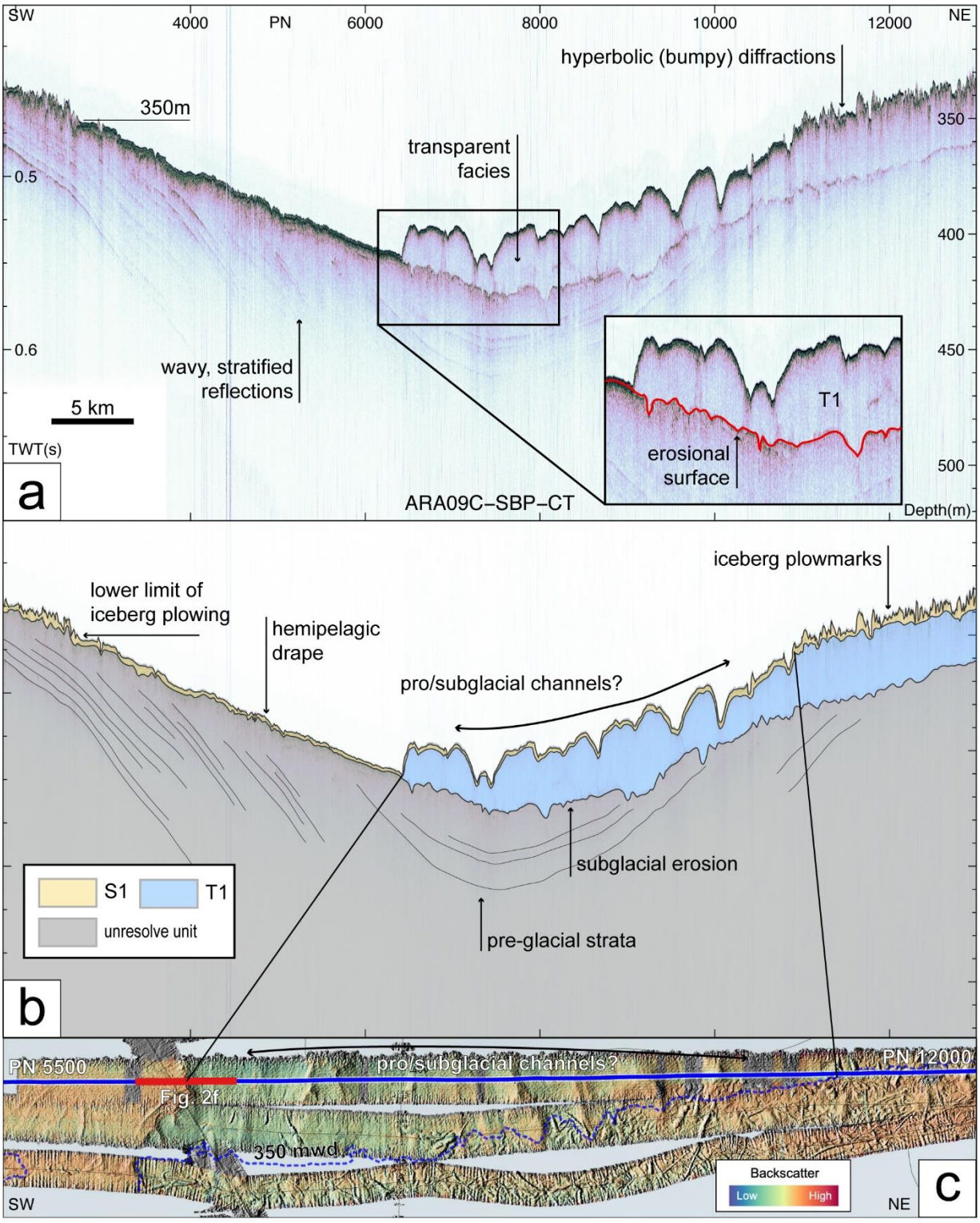

Figure 7. Uninterpreted **(a)** and interpreted **(b)** shelf-edge parallel sub-bottom profile ARA09C-SBP-CT at the northwestern shelf (see Figure 1b for location). The surface of the acoustically transparent deposit T1 features pro- or subglacial channels and iceberg plowmarks at water

depths below and above 350 m, respectively. **(c)** MBES backscatter intensity on the top of T1. Red to blue colors show higher to lower backscatter intensity, respectively.

4.1.2 Seismostratigraphic unit U4

The mapped distribution of U4 shows that a thick (>10 m) stratified portion of the major unit, S4, is widely developed along the upper-mid slope of the western spur and the northwestern margin of the Chukchi Rise (white dashed outlines in Figure 3a). The transparent subunit T4 is characterized by ~5 km wide, 10–20-m-thick accumulations along the upper-mid slope of the margin at water depths of 600–1700 m (Figure 3b). These transparent sediment bodies are intercalated with acoustically stratified sediments (Figure 3b and PN 4800–5800 in Figure 5). Defining the full thickness of the S4 and T4 deposits on the mid-lower southwestern slope is mostly not possible because most of the lower unit boundaries here are not reached by the SBP data (Figure 2d and PN 2300–5300 in Figure 4). Based on the partially observed lower boundaries of S4 and T4 (PN 1800–2300 and 5400–5500 in Figure 4), we determine the thickness of the S4 and T4 deposits as <10 and ~20–70 m, respectively (Figures 3a and 3b). The upper part of U4 in this area shows a distinct lens-shaped, transparent deposit of T4 (Figures 2d and 4). The overall distribution of U4 is restricted to water depths deeper than 600 m (black dashed line in Figures 3a, 3b, and S4a), being possibly eroded at shallower depths, where younger deposits of U2/U1 rest directly on the erosional surface of the unresolved older strata (Figures 6 and 7).

4.1.3 Seismostratigraphic unit U3

The stratified subunit S3 are mostly observed on the continental slope of the northwestern margin and the western spur (Figure 3c), whereas the transparent subunit T3 occupies the southwestern margin at water depths of 550–2100 m (Figure 3d). A 10–20-m-thick accumulation of S3 (white dashed outline in Figure 3c) partially intercalated with transparent lenses of T3 occurs beyond the present-day shelf break (Figure 3d and PN 4800–5000 in Figure 5), similar to the underlying U4 deposits. T3 shows the highest accumulation (>30 m thick, ~70 km wide, white dashed outline in Figure 3d) on the lower slope of the southwestern margin at water depths of 1800–2100 m (Figures 2d and 4). This depocenter can be divided into two depositional bodies interbedded with stratified sediments (Figures 2d and 4b). The upper subunit T3a shows a lens-shaped external geometry and a relatively restricted distribution, whereas, the lower subunit T3b is larger both laterally and vertically and has irregular or sheet-like external geometry (Figure 4). This distinctive stacking pattern of T3 can be observed from the upper to the lower slope of the southwestern Chukchi Rise. T3b is separated from irregularly shaped T4 deposits by a discontinuous, weak reflection (PN 2000–5000 in Figure 4). This faint reflection correlates with the U4/U3 unit boundary in the Chukchi Basin (PN 2000 in Figure 4) and on the lower slope of the western spur (PN 5500 in Figure 4), where acoustic facies are well stratified. On the southwestern outer shelf and upper slope, T3 has a high-amplitude, sub-continuous upper boundary, and a less distinct lower boundary (PN 500–2000 in Figure 6).

4.1.4 Seismostratigraphic unit U2

A thick (>10 m) stratified subunit S2 is widely developed along the slope of the northwestern margin and the western spur and extends to the southwestern margin of the

Chukchi Rise (white dashed outline in Figure 3e). S2 thins out in a basinward direction and reaches a thickness of <10 m in the lower slope (Figure 3e). The internal S2 reflections are generally subparallel to the lower unit boundary of U2 on the mid-lower slope of the southwestern margin and most of the slope at the northwestern margin and the spur (Figure 5).

The main distribution of T2 shows a >20-m-thick, elongated sediment wedge (Figure 6) extending to >80 km along the shelf edge at water depths of 520–640 m (white dashed outline at the shelf edge in Figure 3f) with a downslope extension of debris lobes to 800 mwd (Figure 8a). The wedge at the shelf edge has an uneven lower boundary truncating the stratified internal reflections of the underlying sediments (PN 1700–3000 in Figure 6). The wedge surface is irregular, and the boundary with the overlying stratified sediments of S2/S1 is distinct on the upper slope and shelf edge but gets disturbed further shelfward (PN 4200–5000 in Figure 6 and Figure 8b). Another >20-m-thick, elongated wedge of a similar deposit occurs further shelfward at 300–450 m depths (white dashed outline at the inner shelf in Figure 3f). The stratigraphic relationship between these adjacent deposits is not completely clear, but the presence of an inclined internal reflector (PN 3300–4000 in Figure 8c) indicates that the wedges probably belong to separate depositional events.

A spatially smaller but comparably thick depocenter attributed to T2 is observed on the middle southwestern slope at water depths of 1200–1450 m (Figure 3f). Minor portions of T2 are also distributed on the outer shelf and upper slope of the western spur and the northwestern margin (Figure 3f).

4.1.5 Seismostratigraphic unit U1

The uppermost seismostratigraphic unit U1 features an overall thin (<10 m) stratified subunit S1 along most of the western Chukchi Rise margin (Figure 3g). U1 thins from 5–10 m on the outer shelf to just a couple of meters on the lower slope of the western margin (Figures 2a, 2c, 3g, and S4d). On the outer northwestern shelf, U1 directly overlies the eroded unresolved strata (Figure 7). Transparent facies of T1 cannot be identified in the thin U1 deposits on the mid-lower slope and rise (Figures 3h, 4, and 5), but show a >20-m-thick and >40-km-long sediment wedge at the northwestern shelf edge at water depths of 310–420 m (Figure 3h). This deposit overlies the unresolved strata with an uneven, erosional unconformity, whereas its surface features high-amplitude incisions and furrows, and is covered by a thin (<1–2 m), conformable sedimentary layer (PN 6200–13000 in Figure 7). Minor amounts of transparent deposits occurring on top of the inner T2 wedge on the southwestern margin likely also belong to T1 (PN 2600–4000 in Figure 8c). Thin S1 deposits are observed at <350-mwd throughout the entire study area (PN 1850–2700 and 11000–13000 in Figure 7). The MBES backscatter data on the U1 surface show a sharp intensity variation from –34 to –28 dB on the unresolved, old strata to –42 to –38 dB on the subunit T1 (Figure 7c).

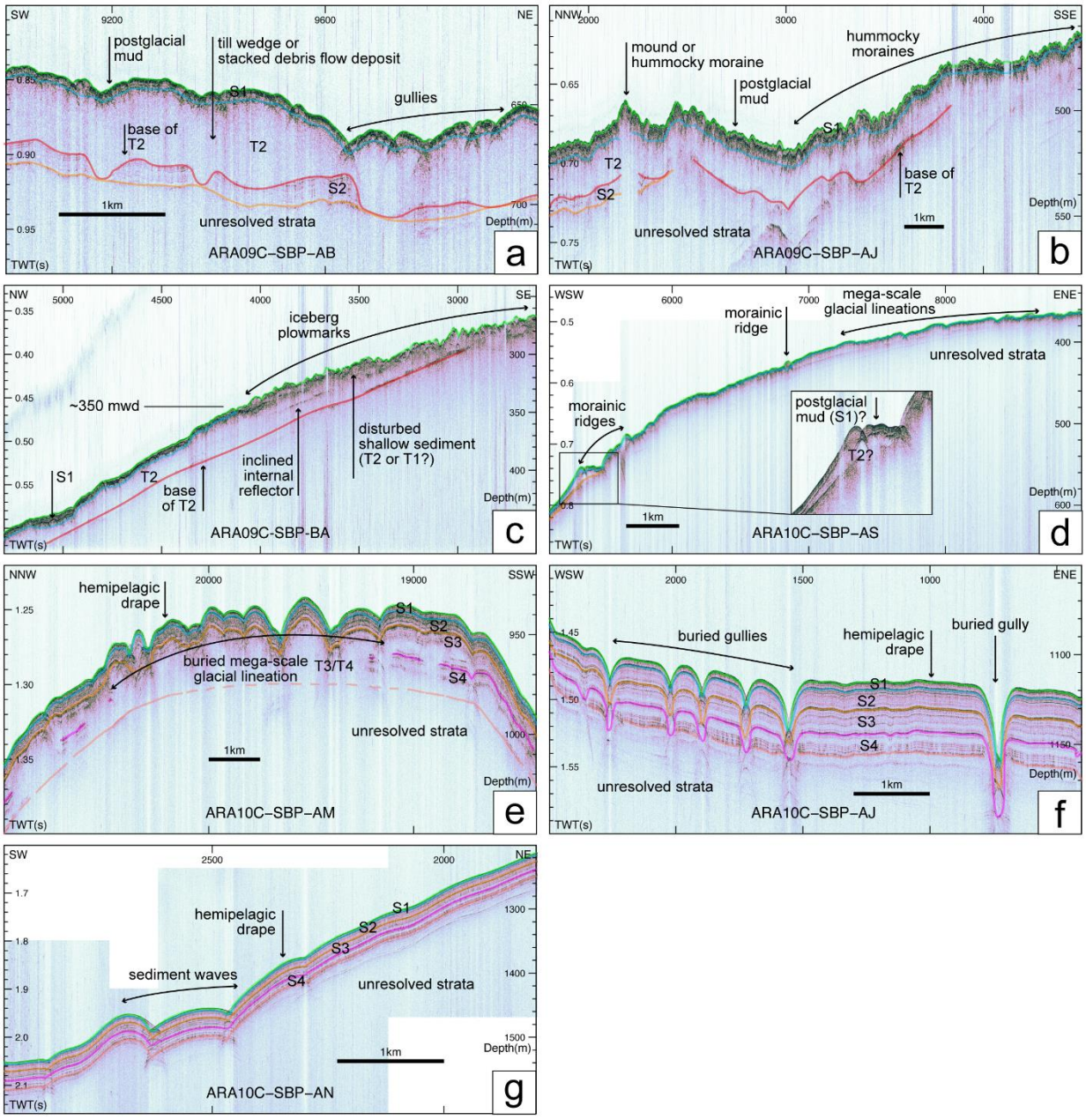

Figure 8. SBP data on the outer shelf to lower slope of the western Chukchi Rise (see Figure 9a for location). **(a)** Gullies on top of the transparent subunit T2 on the upper southwestern slope. **(b)** Mounds and hummocky moraines on the outer southwestern shelf. **(c)** T2 deposits on the southwestern shelf. A faint inclined internal reflector separates two till wedges (Figure 3f). **(d)** Morainic ridges and mega-scale glacial lineations (MSGL) on the outer shelf to upper slope of the western spur. **(e)** Buried MSGLs on the middle slope of the western spur. **(f)** Buried gullies on the northwestern upper-mid slope. Simultaneously acquired airgun seismic data is shown in Figure S2. **(g)** Buried sediment waves on the middle slope of the western spur.

368 ### 4.2 Geomorphic features

369 The MBES bathymetry data provide three-dimensional geometry and detailed
370 morphological characteristics of submarine landforms related to various subglacial, ice-marginal,
371 glaciomarine, and open marine environments (Figures 9 and S5). In addition, the MBES
372 backscatter data can provide indirect characteristics of seabed such as grain-size composition,
373 sediment compaction, and seafloor roughness and hardness (Fransner et al., 2017; Huang et al.,
374 2018; Todd et al., 2007). As the hull-mounted MBES systems have a lower frequency range (12
375 kHz) than usual side-scan sonar systems (550 kHz to 1 MHz), the MBES backscatter data in this
376 study are more suitable for detecting differences in bulk density between young, soft muds and
377 older, consolidated sediments rather than grain size effects (Wille, 2005; Zaragosi et al., 2000).

378 Two sets of streamlined linear landforms are observed in the MBES bathymetry data on
379 the outer shelf and middle slope of the western spur (Figures 8d, 8e, and sky-blue lines in Figure
380 9a). The S–N trending, 5 to 12-km-long and 100 to 200-m-wide lineations on the outer shelf are
381 distributed across a 6-km-wide field at water depths of ~350 to 460 m (Figures 8d and 9a). At the
382 350-mwd limit, lineations are overprinted by the randomly oriented, curvilinear to sinuous
383 furrows 50 to 250-m-wide and <10-m-deep (short black lines in Figure 9a). Both the lineated and
384 furrowed areas have a rough relief appearing in the SBP data as diffraction hyperbolas (e.g., PN
385 11000–13000 in Figure 7a and PN 7200–8700 in Figure 8d). These areas also feature relatively
386 high MBES backscatter of –32 to –28 dB (red-colored field in Figure 9a) and only very thin
387 sediment cover on top (PN 7200–8700 in Figure 8d). The other lineation set features SSW–NNE
388 trending linear features 4 to 7-km-long and 180 to 400-m-wide at water depths of 780 to 940 m
389 on the middle slope (PN 19100–20300 in Figure 8e and Figure 9a). These lineations are formed
390 on top of the transparent subunits T3/T4 and are overlain by 10 to 15-m-thick acoustically
391 stratified sediments S1/S2 with low backscatter intensities of –42 to –34 dB (Figures 8e and 9a).

392 Mostly bathymetry-parallel, nested, curvilinear to sinuous ridges are observed along the
393 shelf edge between 410 and 550-mwd of the western spur and the southwestern Chukchi Rise
394 margin (Figure 8d and blue lines in Figure 9a). Potentially similar, but shorter and sparser
395 features occur on the outer shelf of the southwestern margin, in the area of a >3-km-wide
396 bathymetric terrace (Figure 9a). The ridges on the western spur are 3–6-m-high and >50-km-long
397 along the shelf edge (Figure 9a). The deepest ridge on the western spur shows an asymmetric
398 geometry and is covered by a ~3-m-thick stratified sediments of S1 (inset in Figure 8d). The
399 sparser ridges on the southwestern outer shelf are ~3–5-m-high and ~3–7-km-long (Figure 9a).
400 They are positioned on top of the undulated surface of T2 and are overlain by the stratified
401 sediments of S1 (PN 2200–2700 in Figure 6).

402 Mound-shaped bedforms with transparent acoustic facies are observed on the upper slope
403 and the outer shelf terrace of the southwestern margin at water depths of 600–700-m (inside
404 white dashed outlines in Figure 9a). The mounds are aligned subparallel to the boundary between
405 the western spur and the shelf edge terrace (Figure 9a). Eight mounds surveyed on the upper
406 slope have widths of 200–700 m and are ~10 m higher than the surrounding seafloor (Kim et al.,
407 2020). Larger scale mounds observed on the shelf edge terrace extend stratigraphically to the
408 U2/U1 unit boundary (PN 2100–2500 in Figure 8b and Figure 9a).

409 A field of slightly elongated to nearly circular small mounds (hummocks) is located ~5
410 km shelfward from the shelf break at the southwestern margin at water depths of 440–540 m
411 (inside orange-dashed outline and lower right inset in Figure 9a). This hummocky terrain shows

gentle undulations (<10 m high) and a low-to-moderate linearity. The sediments composing these bedforms belong to the transparent subunit T2 covered by stratified sediments of S1 (PN 3000–4500 in Figure 8b).

Narrow, ~100 m wide, depressions (incisions) in a dip direction are observed along the western Chukchi Rise margin beyond the present-day shelf break at water depths of 600–1600 m (red lines in Figure 9a). The incisions on the southwestern margin are developed on top of the transparent subunit T2 and are covered by ~6-m-thick sedimentary layer S1 (Figure 8a). The depths of these features decrease from ~10–20 m on the shelf break to <10 m on the mid-lower slope. The upper slope incisions disappear on the western spur and are observed again on the northwestern margin (Figure 9a). The latter features of ~20–30-m deep and ~400–500-m wide show a more apparent, less sinuous geometry than on the southwestern slope. A thick (~50 m) acoustically stratified sediment with diffraction hyperbolae covers the area with these incisions (PN 700–800 and 1500–2400 in Figure 8f and Figure S2). Some dip incisions ~7–15-m deep and ~500–1000-m wide were found on the outer shelf of the northwestern margin at 370–400-mwd by the narrow stripes of the MBES data (Figure 7c). The SBP data show that these incisions are developed on top of the transparent subunit T1 (PN 6200–11000 in Figures 7).

Distinctive undulated seafloor features elongated parallel to the bathymetry are observed in the unresolved strata on the middle slope (1300–1600 mwd) at the western spur and the northwestern Chukchi Rise margin (yellow lines in Figures 9a). On the northern slope, these undulated features are cut by downslope incisions (Figures 8f and 9a). A thick (>20 m) stratified sedimentary succession of U4 to U1 conformably overlies the undulating surface (Figure 8g).

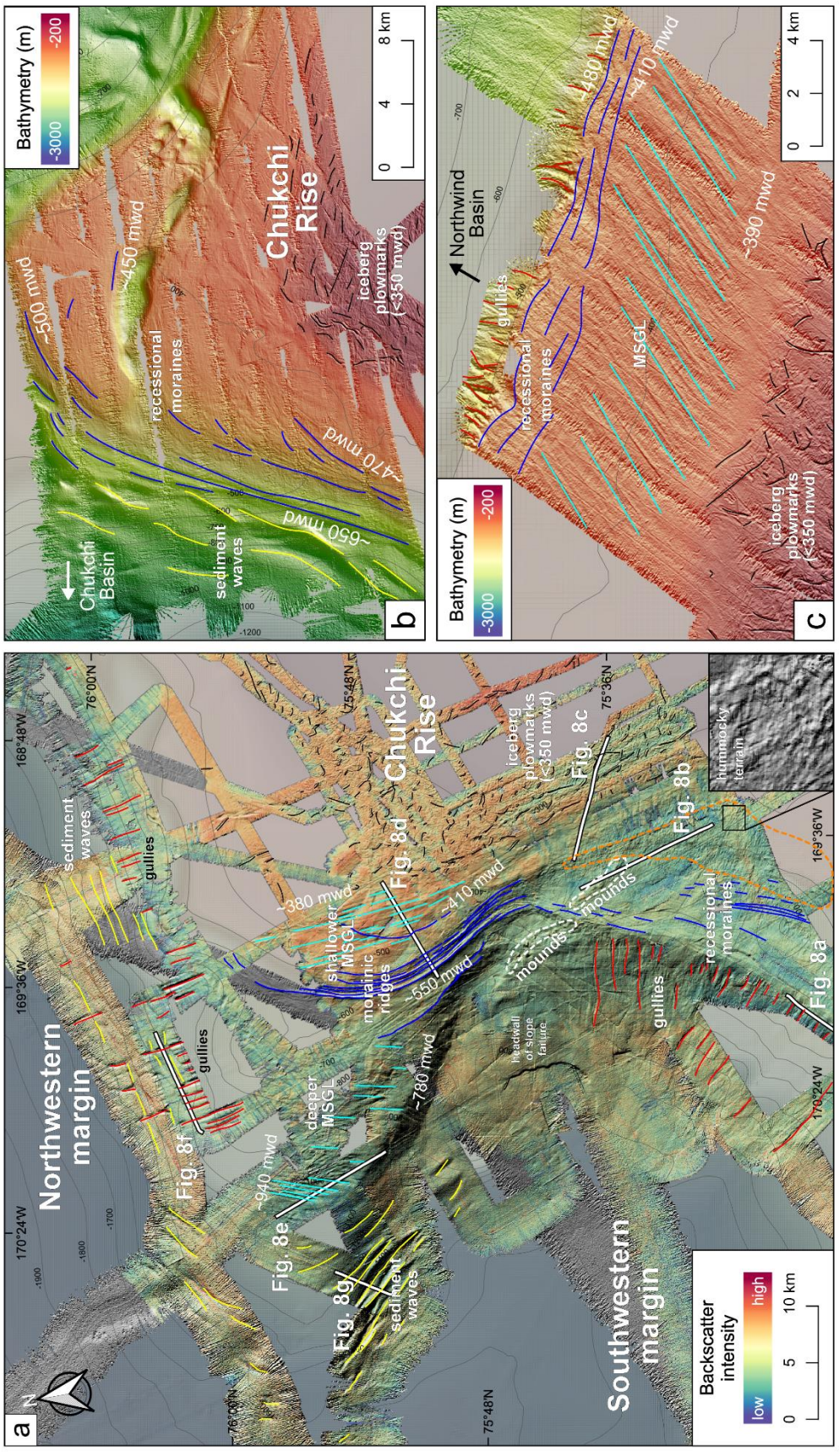
a
Northwestern margin
Southwestern margin
Chukchi Rise
sediment waves
gullies
Fig. 8f
Fig. 8e
Fig. 8g
deeper MSGL
~940 mwd
shallower MSGL
~780 mwd
~380 mwd
Fig. 8d
~410 mwd
~550 mwd
moraine ridges
headwall of slope failure
iceberg plowmarks (<350 mwd)
Fig. 8c
Fig. 8b
mounds
recessional moraines
hummocky terrain
Fig. 8a
Backscatter intensity
low
high
0 5 10 km
b
Bathymetry (m)
-200
-3000
Chukchi Basin
~500 mwd
~450 mwd
recessional moraines
Chukchi Rise
iceberg plowmarks (<350 mwd)
~410 mwd
~650 mwd
sediment waves
0 4 8 km
c
Bathymetry (m)
-200
-3000
Northwind Basin
gullies
~480 mwd
~410 mwd
recessional moraines
MSGL
~390 mwd
iceberg plowmarks (<350 mwd)
0 2 4 km

434

Figure 9. **(a)** Interpreted submarine landforms drawn on the MBES backscatter map overlapping the hillshaded MBES bathymetry map (see Figure S5 for uninterpreted MBES bathymetry image). The interpreted morphological features, which were formed under subglacial, ice-marginal, and glacimarine sub-environments, are marked by differently colored lines and labeled for the explanation. Inset in the lower right corner shows an enlarged view of the hummocky terrain (black box). Labeled white lines show the location of the SBP data in Figures 8a to 8g. Ancillary MBES bathymetry data (ARA03B) from the northern **(b)** and eastern **(c)** parts of the Chukchi Rise (see Figure 1b for location).

5 Discussion

5.1 Origin of identified sedimentary/geomorphic features

5.1.1 Seismostratigraphic units and facies

The major seismostratigraphic boundaries usually indicate either pronounced change in sedimentary environments or depositional unconformities (Veeken & van Moerkerken, 2013). On the glaciated shelves, including the study region (e.g., Dove et al., 2014; Hegewald & Jokat, 2013; Niessen et al., 2013), these features were shown to be characteristically related to the ice-sheet dynamics and associated sedimentary/geomorphic processes. In addition to the direct erosion and deposition by grounded ice, high-amplitude, continuous reflectors commonly occur in glaciomarine environments in connection with massive deposition of iceberg-rafted debris (IRD) during glacial events (Gulick et al., 2017; Joe et al., 2020). In particular, a sediment core–seismic correlation in the western part of the Chukchi Basin indicates that strong reflectors in the SBP data correspond to the prominent, IRD-rich, detrital carbonate layers related to pulses of iceberg discharge from the Laurentide Ice Sheet (Joe et al., 2020).

Seismostratigraphic units/subunits encompassed by the resolved boundaries can be discriminated by the acoustic signature, such as stratified vs. transparent facies (Figure 2). According to previous lithostratigraphic studies, the Quaternary sediments in the western Arctic Ocean outside of the glacially impacted areas mainly consist of fine-grained to sandy muds with cyclic interlamination of brown and yellow to greyish intervals (e.g., Matthiessen et al., 2010; Schreck et al., 2018; Stein et al., 2010). This stratigraphy has been correlated with acoustically stratified facies similar to subunits S4–S1 in areas adjacent to this study area (Dove et al., 2014; Joe et al., 2020; Polyak et al., 2007). A detailed sedimentologic analysis in the western part of the Chukchi Basin indicated that the stratified facies had been formed by suspension settling of turbid meltwater plumes and detached turbid layers during glaciation/deglaciation and by hemipelagic settling during the interglacial periods (Joe et al., 2020). The interpretation is consistent with multiple studies of ice distal glaciomarine sediments (e.g., C. H. Eyles et al., 1991; Ó Cofaigh et al., 2003). In comparison, the transparent deposits (e.g., subunits T4–T1 in Figure 2) indicate lenses of acoustically homogenous sediments without internal bedding due to fast deposition or internal deformation, which is especially common under pro- or subglacial conditions (Alley et al., 1986; Dowdeswell et al., 2004; Gulick et al., 2017). Resulting deposits are seen in the seismic profiles as sheet- or wedge-shaped, acoustically transparent bodies usually interpreted as deformation tills (e.g., Dove et al., 2014; Ó Cofaigh et al., 2005). A similar

acoustic signature may also characterize deposits formed by episodic events like ice-sheet bulldozing, debris flows, submarine landslides, or subglacial underwater flows during the ice-sheet advances or early deglaciations (e.g., Donda et al., 2008; C. H. Eyles & Eyles, 2010; Gales et al., 2016; Joe et al., 2020; Ó Cofaigh et al., 2003; Vorren & Laberg, 1997). However, these short-lived events can hardly account for major, spatially continuous units.

Overall, sediment depocenters and stratal geometries of the acoustically transparent and stratified sediments (Figures 3–7 and 10a) characterize glaciogenic sedimentary processes and provide useful insights into past ice-sheet dynamics. The seismic stratigraphy of the transparent deposits T4–T2 identified at the southwestern margin (Figures 4 to 7) corresponds to the prograding foreset beds with an oblique tangential geometry reported for this area based on the airgun seismic data (Dove et al., 2014; Hegewald & Jokat, 2013; Ilhan & Coakley, 2018) (purple and blue lines in Figure 1b). The outer shelf to slope location, erosional bottom boundary, wedge-shaped stacking pattern, and moderate lateral continuity of these foresets are consistent with seismostratigraphic characteristics of glacial trough mouth fans (TMFs), diamicton-dominated sediment accumulations typically formed at the cross-shelf glacial trough mouth (Batchelor & Dowdeswell, 2014; Dowdeswell et al., 1996; Dowdeswell & Siegert, 1999; Laberg et al., 2000; Ó Cofaigh et al., 2003; Vorren & Laberg, 1997). The occurrence of TMFs at the southwestern Chukchi Rise margin indicates a large amount of sediment transferred by ice sheets to the shelf edge and further down the slope over several glacial cycles. This depositional environment reflects an extensive ice drainage from local or transiting grounded ice-sheets/ice-shelves.

The location of the T4/T3 lens- or sheet-shaped depocenters on the mid-lower slope in the TMF area (Figure 10a) suggests that they have been primarily formed by the glacially-fed debris flows, whereas intercalated stratified facies likely indicate suspension settling from turbid meltwater plumes (Figures 4 and 5). A similar picture has been reported for the East Siberian slope across the Chukchi Basin from the study area (Joe et al., 2020; Niessen et al., 2013). Two T3 subunits separated by the stratified sediments (Figure 4) indicate two depositional events probably reflecting two glacial advances or deglacial pulses.

The T2 depocenter with an erosional basal boundary observed at the outer shelf to upper slope of the Chukchi Rise is interpreted as a till wedge (Figures 6 and 10a). Similar deposits composed of diamictons are typically formed at the stable grounding zones of ice sheets with subglacial sediment transportation and deformation (e.g., Batchelor et al., 2018; Dove et al., 2014; C. H. Eyles & Eyles, 2010; Ó Cofaigh et al., 2016). Based on the position of the large T2 till wedge, during the peak glaciation, the grounding zone was stretched along the shelf break at the modern depths of 550 to 580 mwd (Figure 6; Figure 5 in Dove et al., 2014). A smaller till wedge at depths of ~300–450 m on the southwestern inner shelf (Figures 8c and 10a) possibly indicates another glacial event. The existing data, however, cannot resolve whether this deposit corresponds to T2 or a younger transparent subunit T1. The distribution of the T1 depocenter further north is limited to similar water depths not exceeding ~450 m (Figures 7 and 10a), which suggests that this glaciogenic feature may correspond to the same glaciation. A more detailed characterization of this deposit is not yet available due to a sparse data coverage at the northwestern margin (Figure 1b), notably lacking the shelf-to-slope lines crossing the depocenter.

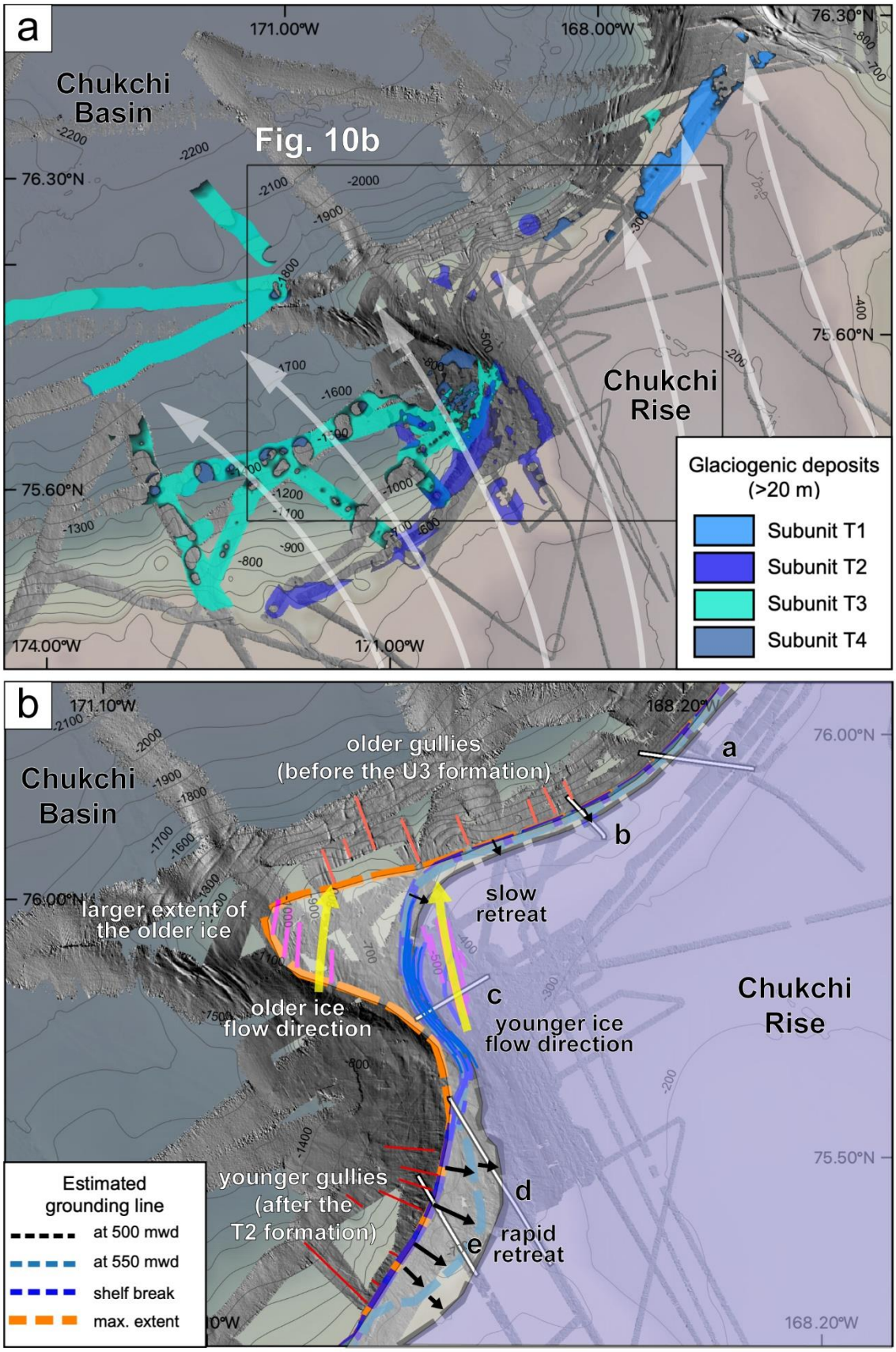
a
Chukchi Basin
Fig. 10b
Chukchi Rise
171.00°W
168.00°W
76.30°N
75.60°N
174.00°W
Glaciogenic deposits (>20 m)
Subunit T1
Subunit T2
Subunit T3
Subunit T4
b
171.10°W
168.20°W
76.00°N
75.50°N
Chukchi Basin
Chukchi Rise
older gullies (before the U3 formation)
larger extent of the older ice
slow retreat
older ice flow direction
younger ice flow direction
younger gullies (after the T2 formation)
rapid retreat
a
b
c
d
e
Estimated grounding line
at 500 mwd
at 550 mwd
shelf break
max. extent

521

Figure 10. **(a)** Spatial distribution of the acoustically transparent deposits T4 to T1 thicker than 20 m. White arrows show major ice-flow trajectories inferred from the distribution of glaciogenic deposits T4 to T1 and related geomorphic features. The black rectangle indicates panel b. **(b)** Distribution of MSGL (purple lines with yellow arrows for the inferred direction), recessional morainic ridges (blue lines), and proglacial gullies (red lines). The orange dashed line indicates the inferred maximum extent of the grounded ice. Blue, sky blue, and black dashed lines are projected grounding lines at the present shelf break, 550 mwd, and 500 mwd, respectively. See also schematic cross-sections for grounding lines projections in Figure S6. Black arrows indicate retreats of grounding-line from the shelf break.

5.1.2 Submarine landforms

The randomly distributed, curvilinear to sinuous furrows abundant at water depths shallower than ~350 m (Figures 9a and 9c) are widely interpreted as iceberg plowmarks generated by the keels of free-floating icebergs under the glaciomarine environment (e.g., Batchelor et al., 2018 and references therein). These features are ubiquitous at <~350-m depths at the outer continental margin from the Canadian Archipelago to East Siberia and the adjacent borderlands (e.g., Dove et al., 2014; Hunkins et al., 1962; Jakobsson et al., 2005, 2008, 2014; Polyak et al., 2001, 2007).

The long, streamlined landforms mapped in two areas of the western Chukchi Rise margin and the ancillary data (Figures 9a and 9c) are identified as mega-scale glacial lineations (MSGL), consistent with the interpretation in multiple studies from the glaciated margins (Dowdeswell et al., 2004; Ottesen et al., 2005). MSGL sets have been reported from multiple sites across the western Arctic Ocean margins and borderlands (Dove et al., 2014; Engels et al., 2008; Jakobsson et al., 2008, 2014, 2016; Niessen et al., 2013; Polyak et al., 2001, 2007). In general, these distinct directional features track the fast ice-stream flows, typically remained during ice-sheet collapses (e.g., Batchelor et al., 2018 and references therein).

By comparison with other glaciated seafloor areas, the bathymetry-parallel ridges at the shelf edge (Figure 9) can be interpreted as recessional moraines formed by the stepwise retreat of a grounded ice margin (Batchelor et al., 2017, 2018; Dove et al., 2014; Niessen et al., 2013; Ottesen & Dowdeswell, 2006; Polyak et al., 1997). The acoustically transparent facies of the identified ridges (inset in Figure 8d) indicate poorly sorted deposits, consistent with the diamict material typical for similar features (Bennett et al., 1996; Bradwell et al., 2008).

The mounds mapped on the southwestern upper slope (Figures 8b and 9a) are thought to be formed by the upward migration of gas/fluids, such as free gas from beneath the gas-hydrate stability zone (Kim et al., 2020). Such processes can be generated or reactivated by pressure and temperature changes in the deep strata caused by glacial isostatic rebounds during the grounded ice-sheet advances and retreats (e.g., Himmler et al., 2019).

The field of small mounds on the southwestern outer shelf has geomorphic and stratigraphic characteristics similar to hummocky moraines (Elvenes & Dowdeswell, 2016; Ottesen & Dowdeswell, 2009) (Figures 8b and 9a). Such landforms can be formed by stagnant ice pressing onto the soft deformable bed over large areas of sub-marginal and proximal

proglacial areas, including submarine environments (e.g., Batchelor et al., 2018 and references therein; Boone & Eyles, 2001; N. Eyles et al., 1999).

The narrow dip incisions at the shelf edge and on the upper-mid slope (Figures 8a, 8f, and 9a) can be interpreted as gullies, which are commonly developed in front of the past ice grounding lines (e.g., Engels et al., 2008; Gales, 2013; Rydningen et al., 2015). On the polar continental margin, slope gullies can result from sustained cascading of cold waters (brines) and/or sediment-laden subglacial meltwater flows (e.g., Anderson, 1999; Ivanov et al., 2004; Lowe & Anderson, 2002; Noormets et al., 2009; Ó Cofaigh et al., 2018; Pope et al., 2018). Broader incisions on top of the youngest transparent deposit T1 on the outer shelf (Figure 7c) may represent valleys formed by the pro- or subglacial drainage during deglaciation (e.g., Stewart & Lonergan, 2011).

The regular undulations elongated along the slope in pre-glacial deposits (Figures 8g and 9a) appear like sediment waves formed by persistent along-slope bottom current (e.g., Miramontes et al., 2016). Similar features can also be identified in the airgun seismic records from the Chukchi margin slopes in the pre-glacial deposits above the upper Miocene unconformity (Hegewald, 2012; Hegewald & Jokat, 2013). A sandy composition of pre-glacial sediments recovered on the northern Northwind Ridge corroborates a strong current activity at the intermediate water depths (Dipre et al., 2018). In comparison, the subparallel stacking pattern of the stratified facies S4 to S1 on top of the sediment waves (Figure 8g) indicates sedimentation in quieter environments less affected by bottom currents (Veeken & van Moerkerken, 2013).

5.2 Development of glaciogenic deposits

5.2.1 Trough mouth fan contributions

Glaciogenic TMFs are typically formed in front of the cross-shelf glacial troughs - elongated, landward deepening bathymetric depressions on the broad continental margins (e.g., Batchelor & Dowdeswell, 2014; Ó Cofaigh et al., 2003). The relatively narrow Chukchi Rise extending offshore from the continental margin makes for a different geomorphic and depositional environment. A slope gradient is considered as one of the principal factors that control the development of TMFs (Batchelor & Dowdeswell, 2014; Ó Cofaigh et al., 2003). The upper slope gradient of the southwestern Chukchi Rise margin is less than 4˚ (2–3˚ average) (Figure 1b), which is suggested to be close to a limit of an effective accumulation of glaciogenic material on the slope (e.g., Batchelor & Dowdeswell, 2014; Piper et al., 2012). Nevertheless, this gradient is considerably higher than 1˚, which allows for well-developed TMFs such as on the Polar North Atlantic margins (e.g., Ó Cofaigh et al., 2003; Piper & Normark, 2009; Rydningen et al., 2015). The acoustically transparent sediment depocenters of subunits T4 and T3 on the southwestern middle to lower slope (Figures 3b, 3d, and 10a) indicate that the gravity-driven mass flow deposits (e.g., submarine landslides and debris flows) largely contributed to the TMF formation by filling the sediment accommodation space in the middle to lower slope, where the slope gradient is less than 1˚ (1100 to 1700 mwd: 0.9˚; 1700 to 2200 mwd: 0.8˚). This infilling may have led to a gradual decrease of the overall slope gradient (e.g., Faleide et al., 1996; O'Grady & Syvitski, 2002), which enabled the accumulation of glaciogenic debris lobes on the gentler slope of the southwestern Chukchi Rise margin. In contrast, a relatively high upper slope gradient (>4˚) of the northwestern Chukchi Rise margin could be a reason for the poorly

developed TMF (e.g., Batchelor & Dowdeswell, 2014; Ó Cofaigh et al., 2003; O'Grady & Syvitski, 2002; Piper & Normark, 2009).

Sediment supply for the TMF formation is also controlled by the subglacial geology of the continental shelf (Batchelor & Dowdeswell, 2014; Halberstadt et al., 2016; Ó Cofaigh et al., 2003, 2004; Solheim et al., 1998; Winsborrow et al., 2010). Prior deep seismostratigraphic data (Figure 1b) show that the pre-glacial strata with laterally continuous internal reflections are widely developed and completely cover high-standing crustal blocks of the Chukchi Rise (Dove et al., 2014; Hegewald & Jokat, 2013; Ilhan & Coakley, 2018). Weakly compacted marine sediment can be much easier eroded by grounded ice rather than crystalline rock or glaciogenic diamicton (e.g., Halberstadt et al., 2016; Moore, 1964; Ó Cofaigh et al., 2003; Wellner et al., 2001; Winsborrow et al., 2010). With respect to TMF development, the seaward-dipping bathymetric trough on the southwestern Chukchi Rise margin (Figure 1b) is relatively less developed than landward-dipping glacial troughs (Batchelor & Dowdeswell, 2014). A seaward-dipping trough can be easily eroded by repeated glacial advances despite a relatively short glacial history, as exemplified by the Mackenzie Trough at the Canadian Arctic margin (Batchelor et al., 2013). We infer that large quantities of sediment on the wide outer shelf of the southwestern Chukchi Rise margin were eroded by the fast-flowing grounded ice and remobilized downslope. This inference is consistent with the occurrence of large-scale glacial sediment T4/T3 depocenters on the mid-lower slope (Figures 4 and 10a).

Suspension settling from turbid meltwater plumes released from an ice-stream front can also contribute to the TMF growth and form gullies on the slope (Gales et al., 2013; Ó Cofaigh et al., 2003; Shipp et al., 1999). The development of gullies varies depending on the upper slope gradient (Klages et al., 2015; Ó Cofaigh et al., 2003). Gullies are weakly developed on the gentle (2 to 3˚) southwestern slope of the Chukchi Rise, whereas deeply incised gullies occur on the steep (>4˚) northwestern slope (Figures 9a and 10b). This distribution implies that the TMF at the southwestern Chukchi Rise margin has been formed by complex sedimentary processes including debris flows and turbid meltwater plumes. Sedimentary deposits from turbid meltwater are characterized by acoustically stratified facies (Joe et al., 2020; Taylor et al., 2002), such as observed in our data between the debris flow packages (e.g., between T3b and T3a in Figure 4).

5.2.2 Glaciogenic facies

Based on the mapped distribution of glaciogenic deposits, major contributions to the TMF at the southwestern Chukchi Rise margin can be attributed to the glacially-fed debris flows of subunits T4/T3 and suspension settling from turbid meltwater plumes forming intercalated stratified facies (Figures 2 to 5). Contributions of T2 are much smaller, although the T2 grounding zone wedge developed on the upper slope and outer shelf, while evidence from older glaciations has not been preserved (Figures 3f and 6). This distribution indicates that the ice sheet that formed T2 had the same or even larger extent than the previous glaciations in this area so that changes in the glaciogenic inputs to the TMF had other controls. In general, the basal thermal condition of an ice-sheet is a major control for sediment transport within a glacial system (Frederick et al., 2016; MacGregor et al., 2016; Menzies & Shilts, 2002). Larger quantities of sediment can be transported under temperate, wet than under cold polar/subpolar basal conditions (Alley et al., 1997; Benn & Evans, 2014; Davis et al., 2006; Kirkbride, 2002; Ottesen et al., 2005; Schomacker et al., 2010; Vorren & Laberg, 1997). In addition, proglacial sedimentation is strongly affected by the volume of meltwater and its proximity to the ice margin

(C. H. Eyles & Eyles, 2010; Menzies & van der Meer, 2018). As a result, faster-flowing ice-sheets with wet-based basal conditions could support more extensive sediment transportation and deposition at larger water depths. Another factor is that during the formation of T4/T3, large volumes of sediments were probably accumulated at the shelf break by subglacial transport of the readily erodible pre-glacial or ice-distal sediments, and subsequently remobilized downslope. In comparison, by the time of the T2 formation, most of the sediment on the outer shelf and upper slope may have been already consumed by the downslope transport. Furthermore, the older strata exposed on the shelf possibly became more compacted by ice-sheet loading (e.g., Böhm et al., 2009).

The continental slope of the western spur and the northwestern Chukchi Rise margin is mainly covered by well-developed stratified sediment layers (S4 to S1) with insignificant lateral variation (Figures 3a, 3c, 3e, and 3g), except for the T1 accumulation at the northwestern outer shelf (Figures 3h and 7). This pattern indicates that gravity-driven mass flow processes were less active here than at the southwestern margin, probably due to colder basal conditions and/or lower sediment fluxes at a more northern location further away from the continental margin. The delivery of sediment to the western spur and the northwestern slope likely occurred mainly by iceberg-rafting and hemipelagic sedimentation, as common for proglacial glaciomarine environments (Ó Cofaigh et al., 2003). The stratified deposits of S4 (or S3 at some sites) to S1 in this area drape the pre-glacial slope features, such as sediment waves and gullies (Figures 8f, 8g, and 9a). This stratigraphy indicates that the active marine down- and along-slope sedimentary processes were diminished since the onset of glaciations when depositional environments became predominantly glaciomarine.

The location of the major T1 glaciogenic depocenter on the outer shelf at relatively shallow water depths of <450 m (Figures 3h and 10a), suggests that T1 was deposited by a smaller and younger ice sheet than T2. Seismostratigraphic correlation of the boundary between U1 and U2 (Figure 2) further indicates that the formation of T1 postdated T2. This evidence is consistent with a lower thickness of acoustically stratified sediment on top of T1 at the northwestern margin (<1 m) than on T2 further south (>5 m) (Figures 3g, 6, and 7), resulting in well-expressed channels on top of T1 (Figures 7c and 10a). In comparison, the T2 surface features a hummocky proglacial moraine and well-developed gas seepage mounds indicative of a stronger glacial impact and/or longer post-glacial period. We note, however, that the thickness of post-glacial sediments depends not only on the time of deposition but also on sediment dynamics. It has been shown for the study region that sedimentation rates since the last major glaciation overall decrease northwards indicating sediment sources further south (Schreck et al., 2018).

5.3 Past ice-sheet dynamics and related processes

The fast-flowing ice streams marked in suitable seafloor sediments by the MSGL are primarily constrained by the ice sheet's mass balance, subglacial topography, and geology (e.g., Halberstadt et al., 2016). In general, the preserved MSGL indicates the latest grounded ice flow just before a final ice retreat, typically by floatation and breakup (e.g., Dowdeswell et al., 2008). The combined MBES and SBP data from the Chukchi Rise indicate that the deeper located (780 to 940 mwd), SSW–NNE oriented MSGL on the middle slope of the western spur were formed prior to the U2 deposits (Figures 8e and 9a). In comparison, N–S oriented MSGL overriding T2

on the outer shelf were clearly formed by a younger and thinner ice mass (Figures 8d and 9a). This interpretation is consistent with the accumulation of acoustically stratified sediments with low backscatter intensity on top of the deeper MSGL, but only a thin sediment cover with higher backscatter intensity on top of the outer shelf MSGL (Figures 8d, 8e, and 9a).

Both MSGL sets occur on a relatively elevated topography, with their general orientation subparallel to the local shelf edge (Figures 9a and 10b), unlike typical MSGL in the cross-shelf glacial troughs (e.g., Batchelor & Dowdeswell, 2014; Dowdeswell et al., 2008; Halberstadt et al., 2016; Shipp et al., 1999). In addition to the lack of a pronounced topographic depression, the distribution of T4 and T3 deposits does not indicate any grounded ice in the MSGL area. This pattern suggests that the MSGL were probably formed by a relatively short-lived, passing ice flow from a thicker ice sheet, potentially formed on the continental margin. The episodic nature of such an ice flow may have been beneficial for MSGL preservation. There is also a possibility that these MSGL could be "plane furrows" produced by huge, tilted tabular icebergs derived from a collapsing ice shelf (Dowdeswell & Bamber, 2007; Wellner et al., 2006). Such furrows are relatively sparse in comparison with the MSGL fields but extend longer with high linearity than typical iceberg plowmarks observed on the Chukchi margin at water depths shallower than ~350 m (Dove et al., 2014) (Figure 9). We note that MSGL and "plane furrows" may co-occur in areas of the past ice-flow/ice-shelf break-up (Wellner et al., 2006).

The sets of laterally extended, isobath-parallel recessional moraines on the outer shelf to upper slope of the western margin are apparently associated mostly with the T2 deposits (Figures 8d and 9a). A prominent stand-alone ridge at shallower water depths of ~400–420 m might indicate a younger glacial event (Figure 9a). This ridge overrides the MSGL in this area and thus was formed after the ice streaming event marked by the MSGL. Overall the ridges likely indicate a stepwise up-slope retreat of the ice-sheet grounding line controlled by the rising sea levels during deglaciation(s) (Batchelor et al., 2018; Jakobsson et al., 2008; Ottesen & Dowdeswell, 2006; Polyak et al., 2001). This pattern contrasts with the bathymetry independent MSGL controlled by the ice-sheet mass balance and topography during ice-sheet collapsing events. The ice-sheet collapses and retreats on the Chukchi Rise may have been triggered by the instability of an ice shelf (shelves) over the adjacent basins in the absence of pinning points (e.g., Halberstadt et al., 2016; Jakobsson et al., 2016; Wellner et al., 2001). Different patterns of the recessional ridge fields on the western spur and the southwestern margin may reflect a lateral variability in the retreat rapidity (Figures 9a and 10b). The western spur features multiple recessional ridges with a high lateral continuity, indicating a relatively gradual, stepwise retreat (e.g., Dowdeswell et al., 2008) (Figures 9a and 10b). The sparser, less developed recessional moraines on the outer-shelf terrace of the southwestern margin possibly indicate a more abrupt retreat of the grounding line from the shelf edge to the inner shelf (Figures 6, 9a, and 10b). The faster retreat may have been facilitated by a deeper shelf break and a flatter gradient of the shelf-edge terrace in the southwestern area (Figures 9a and 10b).

The area of hummocky moraines and mounds developed on the southwestern outer shelf and upper slope is covered by a moderately thick acoustically stratified sediment of S1 with relatively low backscatter intensity (Figures 8b and 9a). This pattern indicates a farther/earlier shelfward retreat of the grounded ice sheet in this area than further north on the western spur and the northwestern margin featuring thinner overlying stratified sediments and higher backscatter intensity (Figures 9a and 10b). The seepage-related mound structures preserved on the outer shelf and upper slope of the southwestern margin also pre-date the U1 deposits (Kim et al., 2020)

(Figure 8b), thus indicating no ice-sheet re-advance in this area after the T2 formation (Figure 10b).

Based on the stratigraphic position of the buried incised surface and the thickness of the overlying acoustically stratified sediments, the gullies on the northwestern slope (Figures 8f and 9a) are probably older (pre-U3) than at the southwestern margin (U2; Figures 8a and 9a). The gully formation can be explained by a grounded ice advance to the shelf edge that provided turbid meltwater pulses capable of incising canyons on the steep slope (Lowe & Anderson, 2003; Ó Cofaigh et al., 2003). After the gully formation event at the northwestern slope, no sufficient sediment-laden meltwater was generated in this area, possibly due to a change in the basal thermal condition from the temperate-wet to the polar-cold (Rebesco & Camerlenghi, 2008). The younger and smaller gullies on the southwestern slope indicate overall lower amounts of subglacial meltwater discharged during the T2 glacial event. In comparison to the deeper located slope gullies, the fresh-looking, relatively shallow but broad (up to 1000 m) channels on top of the T1 wedge on the northwestern shelf likely have a different nature. Considering their geometry and the position on a gently dipping surface of the youngest glacial deposit, they may be related to the subglacial drainage at the final deglacial stages. On the other hand, low backscatter intensities of the T1 wedge surface (Figure 7c) are more common for proglacial rather than subglacial deposits. Clarifying the nature of this glaciogenic accumulation requires denser data coverage, including shelf-to-slope lines. Buried valleys reaching considerably larger dimensions are widely distributed across the Chukchi margin (Dove et al., 2014; Hill et al., 2007; Hill & Driscoll, 2008). Their common occurrence on the Chukchi Rise at water depths of >300 m indicates their subglacial rather than river-born origin (Dove et al., 2014).

The pre-glacial sediment waves expressed in bathymetry-parallel, undulating morphology are well preserved on the slope of the western spur and the northwestern margin due to the conformable geometry of the overlying acoustically stratified deposits of S4–S1 (Figure 8g). The absence of similar undulations on the southwestern slope (Figure 9a) can be explained by the burial of pre-glacial sediment waves by the thick TMF deposits (Dove et al., 2014; Hegewald & Jokat, 2013; Ilhan & Coakley, 2018).

5.4 Glaciation history

5.4.1 Ice-sheet distribution and provenance

The overall distribution of glaciogenic seafloor morphology and sediment stratigraphy in the study area is consistent with the notion that Arctic ice sheets advanced from the continental margins toward the central Arctic Ocean and retreated upslope back to the margins and shallow bathymetric areas (Dove et al., 2014; Engels et al., 2008; Jakobsson et al., 2008, 2010, 2014; Polyak et al., 2001, 2007). If the entire Arctic Ocean was covered by a thick ice shelf during some of the peak glaciations, it likely behaved as a single large ice mass outflowing into the North Atlantic (Hughes et al., 1977; Jakobsson et al., 2016). Due to these changes in ice flow and a lack of major topographic constraints, such as cross-shelf troughs or inter-island channels, the directions of ice advances and retreats at the western Chukchi Rise margin are more complex than on the well-developed glaciated margins around the Antarctic, Polar North Atlantic, and the Canadian Arctic Archipelago (Batchelor et al., 2014; Batchelor & Dowdeswell, 2014; Halberstadt et al., 2016; Ó Cofaigh et al., 2003; Winsborrow et al., 2010).

Prior MBES data from the Chukchi Borderland collected mostly east of the study area indicate a prevalent SE–NW to ESE–WNW trending impact of grounded ice mass(es) projected to originate from the northwestern sector of the Laurentide Ice Sheet (Figure 1a) (Dove et al., 2014; Engels et al., 2008; Jakobsson et al., 2008, 2014; Polyak et al., 2001, 2007). Another distinct set of directional seafloor features on the eastern side of the Chukchi Rise appears to irradiate from the Chukchi Shelf (Dove et al., 2014; Jakobsson et al., 2014), as also observed in our ancillary data (Figure 9c). The co-occurrence of these major flowline trends makes a complex picture reflecting the interaction of different ice flows. The evidence for ice provenance in our seismostratigraphic and geomorphic data from the western side of the Chukchi Rise provides another important piece for this puzzle picture.

Based on the TMF location in the seaward-dipping bathymetric trough at the southwestern Chukchi Rise margin and the distribution of glaciogenic deposits T4/T3 preserved on the slope, the general ice flow direction in this area was probably northwestward from the Chukchi Shelf toward the Chukchi Basin (Figure 10a). A similar, more S–N orientation of an MSGL set on the outer shelf formed apparently on top of T2 (Figure 9a) also suggests an ice flow from the Chukchi margin. The prominent grounding zone till wedges on the western margin at the shelf edge and further shelfward probably mark standstill positions of the grounded ice margins (Figure 10b). The up-slope deglacial retreat of the ice margins is marked by sets of recessional moraines (Figure 8d, 9a, and 10b), also observed at the northern Chukchi Rise tip (Figure 9b) and in prior data from the Chukchi Rise and Cap further east and north (Dove et al., 2014; Jakobsson et al., 2008). In our data, these ridges appear to be primarily associated with T2. Similar grounding zone standstill and retreat features for T4/T3 apparently have not been preserved.

The overall picture emerging from these data indicates that ice coming from the Laurentide Ice Sheet may have been deflected northwards (i.e., towards the Canada Basin) by the ice sheet(s) irradiating from the Chukchi margin. Alternatively, it can also be inferred that the younger Chukchi-centered ice sheets overprinted the depositional/geomorphic evidence of the older ice masses with different flow trajectories. Considering that our data cover four glacial intervals with a long glacial history, it is more likely that coeval ice masses with different provenance actually interacted on the Chukchi Rise. We note that while multiple seafloor features indicate ice flow(s) from the Chukchi continental margin, they cannot be confirmed by data from the shelf itself (Dove et al., 2014; Jakobsson et al., 2014). The obvious reason for this lack of evidence is that sedimentary bedforms cannot preserve on the shallow, current-swept Chukchi Shelf. Deeper geophysical records and drilling boreholes are needed to resolve this gaping blind spot.

On the western side of the Chukchi Rise, the ice-flow interactions can also be envisaged with the East Siberian Ice Sheet. While still sketchily understood, this ice sheet is corroborated by multiple seafloor data (Jakobsson et al., 2016; Joe et al., 2020; Niessen et al., 2013; O'Regan et al., 2017; Schreck et al., 2018) and paleoclimatic modeling studies (Colleoni et al., 2016; Gasson et al., 2018). If the ice shelves extending from the East Siberian and Chukchi margins consequently coalesced and started to behave like a single large ice mass (Hughes et al., 1977; Jakobsson et al., 2016), the flow direction would have been re-oriented towards the central Arctic Ocean, orthogonally to the Chukchi–East Siberian margin. This orientation may have accounted for the SSW–NNE trending, deep-sited MSGL on top of the T3 deposits on the western spur (Figure 10b). The large water depth of these features (>900 m) is similar to the ice

grounding on the Lomonosov Ridge in the center of the Arctic Ocean (Jakobsson et al., 2001, 2008, 2010, 2014; Polyak et al., 2001). Elaborating these mechanisms is important for understanding the behavior of the Arctic glaciations and, more generally, the large marine-based ice complexes.

5.4.2 Age framework

While there are no direct constraints for the age of the mapped glaciogenic deposits, a tentative age framework can be outlined from stratigraphic data available from the adjacent areas (Dipre et al., 2018; Joe et al., 2020; Polyak et al., 2007; Schreck et al., 2018; Wang et al., 2013). In particular, combined geological/geophysical data from the southeastern part of the Chukchi Borderland (ramp to the Northwind Ridge; Figure 1b) provide age constraints for the last two glacial events impacting this seafloor area (Polyak et al., 2007). Glacial diamicton dated to the Last Glacial Maximum (LGM) of the Marine Isotope Stage (MIS) 2, ca. 15–25 ka, is associated with the W–E trending MSGL at modern water depths to ~420–430 m. A nearby MSGL field mapped at the southeastern side of the Chukchi Rise and presented in this study has similar bathymetric and geomorphic characteristics (Figures 1b and 9c). The MSGL orientations in these two fields indicate ice streaming from the Chukchi margin. This picture is consistent with the distribution of the T1 deposits at the western Chukchi Rise, which is restricted to water depths of <450 m and are covered with only thin post-glacial sediments (Figures 3h, 7, and 10a). Well-expressed channels on top of the T1 deposit at the northwestern shelf possibly represent the pro- or subglacial drainage during deglaciation, similar to, but younger than buried valleys reported for the Chukchi Rise by Dove et al. (2014). These characteristics of the T1 deposits allow for attribution of their formation to the LGM. This interpretation is also consistent with sediment-core evidence from the Chukchi Basin that suggests the presence of the LGM grounded ice masses at shallower depths in this region (Joe et al., 2020; Schreck et al., 2018; Wang et al., 2013).

Glacial deposits attributed to MIS 4 (ca. 60–70 ka) appear to be widely distributed in the study region, including tills on the bathymetric highs, debris lobes on the slopes, and thick glaciomarine deposits in the basins (Joe et al., 2020; Polyak et al., 2007; Schreck et al., 2018; Wang et al., 2013). The corresponding glaciogenic bedforms such as MSGL and morainic ridges extend to the shelf edge at ~600–700 mwd (Dove et al., 2014; Jakobsson et al., 2008; Polyak et al., 2007). At the southern Northwind Ridge, these deposits feature the SE–NW trending MSGL indicative of an ice flow from the Laurentide Ice Sheet (Polyak et al., 2007). MSGL with a similar orientation and depth range are also widely reported elsewhere from the Northwind Ridge, Chukchi Cap, and Alaskan margin (Dove et al., 2014; Engels et al., 2008; Jakobsson et al., 2005, 2008). The seismostratigraphic and bathymetric position of the T2 deposits indicates their probable relation to the co-eval glacial event. The seismostratigraphic boundaries of U2, including T2 (H2/H3, Figure 2a), apparently correspond to reflectors R2/R3 defined for the East Siberian (Arliss Plateau) slope across the Chukchi Basin (Joe et al., 2020). These reflectors were related to prominent IRD layers formed by the iceberg discharge pulses from the Laurentide Ice Sheet during the deglaciations following and preceding MIS 4. Despite probable synchronicity with a Laurentide-sourced ice advance inferred for more eastern areas, this glaciation on the western Chukchi Rise apparently had a different provenance based on the S–N-trending orientation of the MSGL on top of T2. According to this orientation, the main grounded ice was located south of the Chukchi Rise at least at the late glacial stages. This inference is consistent with the formation of a hummocky moraine south of the MSGL field (Figure 9a).

The age controls for the older glacial deposits T4/T3 preserved in the study area only as debris lobes on the slope are more speculative. The potentially largest glacial impact in the Arctic has been inferred for MIS 6 (late Middle Pleistocene, ca. 130–190 ka) based on a very deep (>1 km) ice grounding on the Lomonosov Ridge in the center of the Arctic Ocean constrained to this glacial interval (Jakobsson et al., 2001, 2010, 2014, 2016; Polyak et al., 2001). Reconstructed circum-Arctic ice-sheet limits also show a very large extent for the northern North America and the largest for the northern Eurasia (Batchelor et al., 2019 and references therein). Glacial diamicton probably of this age has been recovered on top of the northern part of the Northwind Ridge in front of a prominent morainic ridge (Dipre et al., 2018; Jakobsson et al., 2010). A large pre-MIS 4 debris lobe on the East Siberian slope (Arliss Plateau: Joe et al., 2020) may also belong to the MIS 6. A possible attribution of the glaciogenic T3 deposits to this glaciation is indirectly supported by the MSGL set formed at water depths to >900 m on top of T3 and aligned with the direction towards the central Arctic Ocean (Figures 9a and 10). Two glaciogenic lobes identified as subunits of T3 (Figure 4) indicate two glacial events, possibly stages of the same glaciation.

The age of the oldest glaciogenic unit T4 can be considered in relation to the history of a large-scale glacial erosion on the Chukchi margin/borderland. Based on regional airgun seismic data, the glaciogenic erosional boundary occurs on top of deposits overlying the late Miocene unconformity and is broadly attributed to Plio-Pleistocene (Hegewald, 2012; Hegewald & Jokat, 2013; Ilhan & Coakley, 2018). In sediment cores from the northern Northwind Ridge the contact between pre-glacial and glaciogenic strata is constrained by cyclostratigraphy and strontium isotope dating to MIS 16/20, ca. 0.7–0.9 Ma (Dipre et al., 2018; Polyak et al., 2013). This timing corresponds to a prominent change in paleoclimatic conditions (Mid-Pleistocene Transition) related to a shift in the prevailing orbital cyclicities and the development of huge ice sheets in the Northern Hemisphere in the Middle Pleistocene starting with MIS 16 (Clark et al., 2006; Lisiecki & Raymo, 2005).

Based on the airgun seismic data, there is one glaciogenic sedimentary package between the reflector H5 (lower boundary of unit U4) and the initial glaciogenic unconformity (Dove et al., 2014) (H6; Figure S3). This stratigraphy indicates that T4 was formed during the second regional glacial event. If the first glacial expansion occurred in MIS 16 or somewhat earlier, the T4 age can be placed somewhere in the lower part of the Middle Pleistocene, such as MIS 12 that was a prominent glaciation based on a sedimentary record from the Canada Basin (Dong et al., 2017).

Constraining the outlined stratigraphic estimates more conclusively requires more sediment cores, preferably with long records such as pursued by the International Ocean Discovery Program (IODP). Our data may contribute useful information for developing an IODP project in the Chukchi region.

6 Summary and conclusions

This study presents the detailed, high-resolution sub-bottom profiler (SBP) and multibeam echosounder (MBES) data from the Chukchi Rise in the western Arctic Ocean. The combined seismostratigraphic and morphobathymetric analysis sheds new light on the past ice-sheet/ice-shelf distribution and dynamics and related sedimentary/geomorphic processes. Results

of this study provide important empirical constraints for reconstructing Quaternary glaciations in and around the Arctic Ocean.

Based on the acoustic character of sediments revealed by the SBP data, we identify four seismostratigraphic units, U4–U1, each including acoustically stratified and transparent facies classified as subunits S4–S1 and T4–T1, respectively. The transparent facies are interpreted as glaciogenic sediments deposited during glacial events probably spanning most of the Middle to Late Pleistocene (ca. 0.5–1 Ma). The older transparent deposits (T4/T3) are preserved on the southwestern mid-lower slope of the Chukchi Rise as debris lobes contributing to a large trough mouth fan identified on the regional airgun seismic records. On the upper slope to outer shelf, these features are replaced by a younger, wedge- to sheet-shaped deposit (T2) with an erosional lower boundary and glaciogenic bedforms at the surface, such as mega-scale glacial lineations (MSGL), recessional morainic ridges, and hummocky moraines. The main T2 deposit at the shelf break is interpreted as a glacial grounding zone wedge possibly formed during MIS 4 (ca. 60–70 ka). The youngest transparent deposit (T1), attributed to the Last Glacial Maximum (MIS 2, ca. 15–25 ka), occurs on the outer shelf at shallower water depths.

Two mapped sets of MSGL trending SSW–NNE on top of T3 on the middle slope and S–N on T2 on the outer shelf demonstrate at least two fast ice-streaming events of different ages. The older, deeper sited (ca 780–940 mwd) MSGL may be related to a passage of a large ice shelf formed over the western Arctic Ocean. Contour-parallel, nested recessional-moraine ridges are identified along the outer shelf to upper slope on top of the grounding zone deposits. Correlative ridges are also mapped north of the main study area, thus indicating their distribution along the entire Chukchi Rise margin. The well-developed ridges mark a stepwise retreat of the grounded ice margin, likely controlled by rising sea levels during deglaciation(s). More random ridges at a flatter bathymetric bench on the southwestern margin may indicate a faster retreat. The different orientations of ice advances and retreats reflect a complex geomorphic setting of the borderland that lacks major topographic controls typical for glaciated continental margins, such as cross-shelf glacial troughs.

The seismostratigraphic and geomorphic data suggest that ice flow directions for all of the identified glacial events were principally from the Chukchi continental margin south of the study area. Based on the additional mapping and prior data, the same ice-sheet origin can be projected for glaciogenic bedforms on the eastern side of the Chukchi Rise, along with the evidence of ice flow(s) apparently originating from the northwestern Laurentide Ice Sheet. This complex picture shows that the Chukchi Rise was an area of intense interaction(s) of different ice-sheets/ice-shelves that affected the overall glaciation development in the Arctic Ocean.

In addition to glaciogenic deposits and bedforms, our data identify a number of related or independent seabed features including mounds, gullies/channels, and sediment waves. Mounds, presumably formed by gas seepage, grow from the surface of the T2 deposit, possibly triggered by glaciogenic pressure effects. Buried gullies on the upper slope were likely incised by proglacial turbid water flows, while fresh-looking, broad channels on top of the T1 deposit on the shelf may be related to the pro- or subglacial drainage during the last deglaciation. Sediment waves are characteristic for pre-glacial sediments on the middle slope, thus indicating active hydrodynamic conditions at the intermediate water depths before the onset of major glaciations.

Acknowledgments

The authors are grateful to the captain and crew of the IBRV *Araon* for their help provided during the Arctic expeditions since 2012. This work was supported by the Korea Polar Research Institute (KOPRI) Grant PM20050 (KIMST Grant 20160247). Y. J. Joe and S.-I. Nam acknowledge funding from the KOPRI Grant PE20350. F. Niessen was funded by the AWI Research Program PACES-II, Workpackages 3.1 and 3.2. We thank SeisWare Inc. for the academic grant program for using the software for seismostratigraphic analysis and mapping. SBP data processing, MBES data gridding, and mapping were conducted using the open-source software Seismic Unix (https://wiki.seismic-unix.org), Generic Mapping Tools (https://www.generic-mapping-tools.org), and QGIS (https://qgis.org). The MBES bathymetry/backscatter and units/subunits thickness mapping results used in this study are archived by the Korea Polar Data Center and are available at https://kpdc.kopri.re.kr.

Appendix A. Supplementary data

Supplementary data to this article can be found online at "https://dx.doi.org/doi:10.22663/KOPRI-KPDC-00001625.1".

References

Alley, R. B., Blankenship, D. D., Bentley, C. R., & Rooney, S. T. (1986). Deformation of till beneath ice stream B, West Antarctica. *Nature*, (6074), 57–59.

Alley, R. B., Cuffey, K., Evenson, E., Strasser, J., Lawson, D., & Larson, G. (1997). How glaciers entrain and transport basal sediment: physical constraints. *Quaternary Science Reviews*, *16*(9), 1017–1038. https://doi.org/10.1016/S0277-3791(97)00034-6

Anderson, J. B. (1999). *Antarctic marine geology* (Vol. 289). Cambridge Univ Press.

Batchelor, C. L., & Dowdeswell, J. A. (2014). The physiography of High Arctic cross-shelf troughs. *Quaternary Science Reviews*, *92*, 68–96. http://dx.doi.org/10.1016/j.quascirev.2013.05.025

Batchelor, C. L., Dowdeswell, J. A., & Pietras, J. T. (2013). Seismic stratigraphy, sedimentary architecture and palaeo-glaciology of the Mackenzie Trough: evidence for two Quaternary ice advances and limited fan development on the western Canadian Beaufort Sea margin. *Quaternary Science Reviews*, *65*, 73–87. http://dx.doi.org/10.1016/j.quascirev.2013.01.021

Batchelor, C. L., Dowdeswell, J. A., & Pietras, J. T. (2014). Evidence for multiple Quaternary ice advances and fan development from the Amundsen Gulf cross-shelf trough and slope, Canadian Beaufort Sea margin. *Marine and Petroleum Geology*, *52*, 125–143. http://dx.doi.org/10.1016/j.marpetgeo.2013.11.005

Batchelor, C. L., Ottesen, D., & Dowdeswell, J. A. (2017). Quaternary evolution of the northern North Sea margin through glacigenic debris-flow and contourite deposition. *Journal of Quaternary Science*, *32*(3), 416–426. https://doi.org/10.1002/jqs.2934

Batchelor, C. L., Dowdeswell, J. A., & Ottesen, D. (2018). Submarine Glacial Landforms. In A. Micallef, S. Krastel, & A. Savini (Eds.), *Submarine Geomorphology* (pp. 207–234). Cham: Springer International Publishing. https://doi.org/10.1007/978-3-319-57852-1_12

Batchelor, C. L., Margold, M., Krapp, M., Murton, D. K., Dalton, A. S., Gibbard, P. L., et al. (2019). The configuration of Northern Hemisphere ice sheets through the Quaternary. *Nature Communications*, *10*(1), 3713. https://doi.org/10.1038/s41467-019-11601-2

Benn, D., & Evans, D. J. (2014). *Glaciers and glaciation* (Second). Hodder Education.

Bennett, M. R., Huddart, D., Hambrey, M. J., & Ghienne, J. F. (1996). Moraine Development at the High-Arctic Valley Glacier Pedersenbreen, Svalbard. *Geografiska Annaler: Series A, Physical Geography*, *78*(4), 209–222. https://doi.org/10.1080/04353676.1996.11880468

Böhm, G., Ocakoğlu, N., Picotti, S., & De Santis, L. (2009). West Antarctic Ice Sheet evolution: New insights from a seismic tomographic 3D depth model in the Eastern Ross Sea (Antarctica). *Marine Geology*, *266*(1), 109–128.

Boone, S. J., & Eyles, N. (2001). Geotechnical model for great plains hummocky moraine formed by till deformation below stagnant ice. *Geomorphology*, *38*(1), 109–124. https://doi.org/10.1016/S0169-555X(00)00072-6

Bradwell, T., Stoker, M. S., Golledge, N. R., Wilson, C. K., Merritt, J. W., Long, D., et al. (2008). The northern sector of the last British Ice Sheet: Maximum extent and demise. *Earth-Science Reviews*, *88*(3), 207–226. https://doi.org/10.1016/j.earscirev.2008.01.008

Clark, P. U., Archer, D., Pollard, D., Blum, J. D., Rial, J. A., Brovkin, V., et al. (2006). The middle Pleistocene transition: characteristics, mechanisms, and implications for long-term changes in atmospheric pCO2. *Quaternary Science Reviews*, *25*(23), 3150–3184. https://doi.org/10.1016/j.quascirev.2006.07.008

Coakley, B. J., Ilhan, I., & Chukchi Edges Science Party. (2011). Chukchi Edges Project-Geophysical constraints on the history of the Amerasia Basin. In *AGU Fall Meeting Abstracts* (Vol. 1, p. 2365).

Colleoni, F., Kirchner, N., Niessen, F., Quiquet, A., & Liakka, J. (2016). An East Siberian ice shelf during the Late Pleistocene glaciations: Numerical reconstructions. *Quaternary Science Reviews*, *147*(Special Issue: PAST Gateways (Palaeo-Arctic Spatial and Temporal Gateways)), 148–163.

Darby, D. A., Jakobsson, M., & Polyak, L. (2005). Icebreaker expedition collects key Arctic seafloor and ice data. *Eos, Transactions American Geophysical Union*, *86*(52), 549–552.

Davis, P. T., Briner, J. P., Coulthard, R. D., Finkel, R. W., & Miller, G. H. (2006). Preservation of Arctic landscapes overridden by cold-based ice sheets. *Quaternary Research*, *65*(1), 156–163. https://doi.org/10.1016/j.yqres.2005.08.019

DeConto, R. M., & Pollard, D. (2016). Contribution of Antarctica to past and future sea-level rise. *Nature*, *531*(7596), 591–597.

Dipre, G. R., Polyak, L., Kuznetsov, A. B., Oti, E. A., Ortiz, J. D., Brachfeld, S. A., et al. (2018). Plio-Pleistocene sedimentary record from the Northwind Ridge: new insights into paleoclimatic evolution of the western Arctic Ocean for the last 5 Ma. *Arktos*, (1), 24.

Donda, F., O'Brien, P., De Santis, L., Rebesco, M., & Brancolini, G. (2008). Mass wasting processes in the Western Wilkes Land margin: possible implications for East Antarctic glacial history. *Palaeogeography, Palaeoclimatology, Palaeoecology*, *260*(1), 77–91.

Dong, L., Liu, Y., Shi, X., Polyak, L., Huang, Y., Fang, X., et al. (2017). Sedimentary record from the Canada Basin, Arctic Ocean: implications for late to middle Pleistocene glacial history. *Climate of the Past*, *13*(5), 511–531. https://doi.org/10.5194/cp-13-511-2017

Dove, D., Polyak, L., & Coakley, B. J. (2014). Widespread, multi-source glacial erosion on the Chukchi margin, Arctic Ocean. *Quaternary Science Reviews*, *92*, 112–122.

Dowdeswell, J. A., & Bamber, J. L. (2007). Keel depths of modern Antarctic icebergs and implications for sea-floor scouring in the geological record. *Marine Geology*, *243*(1), 120–131.

Dowdeswell, J. A., & Siegert, M. J. (1999). Ice-sheet numerical modeling and marine geophysical measurements of glacier-derived sedimentation on the Eurasian Arctic continental margins. *Geological Society of America Bulletin*, *111*(7), 1080–1097.

Dowdeswell, J. A., Kenyon, N., Elverhøi, A., Laberg, J., Hollender, F., Mienert, J., & Siegert, M. (1996). Large-scale sedimentation on the glacier-influenced Polar North Atlantic margins: long-range side-scan sonar evidence. *Geophysical Research Letters*, *23*(24), 3535–3538.

Dowdeswell, J. A., Cofaigh, C. Ó., & Pudsey, C. J. (2004). Thickness and extent of the subglacial till layer beneath an Antarctic paleo–ice stream. *Geology*, *32*(1), 13–16.

Dowdeswell, J. A., Ottesen, D., Evans, J., Cofaigh, C. Ó., & Anderson, J. (2008). Submarine glacial landforms and rates of ice-stream collapse. *Geology*, *36*(10), 819–822.

Dowdeswell, J. A., Canals, M., Jakobsson, M., Todd, B. J., Dowdeswell, E. K., & Hogan, K. A. (2016). *Atlas of Submarine Glacial Landforms: Modern, Quaternary and Ancient*. (J. A. Dowdeswell, M. Canals, M. Jakobsson, B. J. Todd, E. K. Dowdeswell, & K. A. Hogan, Eds.) (Vol. 46). Geological Society of London.

Elvenes, S., & Dowdeswell, J. A. (2016). Possible "lift-off moraines" at grounded ice-sheet margins, North Norwegian shelf edge. *Geological Society, London, Memoirs*, *46*(1), 247–248.

Elverhøi, A., Dowdeswell, J. A., Funder, S., Mangerud, J., & Stein, R. (1998). Glacial and oceanic history of the Polar Nnorth Atlantic Margins: An Overview. *Quaternary Science Reviews*, *17*(1), 1–10. http://dx.doi.org/10.1016/S0277-3791(97)00073-5

Engels, J. L., Edwards, M. H., Polyak, L., & Johnson, P. D. (2008). Seafloor evidence for ice shelf flow across the Alaska–Beaufort margin of the Arctic Ocean. *Earth Surface Processes and Landforms*, *33*(7), 1047–1063. https://doi.org/10.1002/esp.1601

Eyles, C. H., & Eyles, N. (2010). Glacial deposits. In *Facies Models 4* (pp. 73–104). The Geological Association of Canada'.

Eyles, C. H., Eyles, N., & Lagoe, M. B. (1991). The Yakataga Formation: A six million year record of temperate glacial marine sedimentation in the Gulf of Alaska. In J. B. Anderson & G. M. Ashley (Eds.), *Glacial Marine Sedimentation: Paleoclimatic Significance* (Vol. 261, pp. 159–180). Geological Society of America.

Eyles, N., Boyce, J. I., & Barendregt, R. W. (1999). Hummocky moraine: sedimentary record of stagnant Laurentide Ice Sheet lobes resting on soft beds. *Sedimentary Geology*, *123*(3), 163–174. https://doi.org/10.1016/S0037-0738(98)00129-8

Faleide, J. I., Solheim, A., Fiedler, A., Hjelstuen, B. O., Andersen, E. S., & Vanneste, K. (1996). Late Cenozoic evolution of the western Barents Sea-Svalbard continental margin. *Global and Planetary Change*, *12*(1), 53–74.

Fransner, O., Noormets, R., Flink, A. E., Hogan, K. A., & Dowdeswell, J. A. (2017). Sedimentary processes on the continental slope off Kvitøya and Albertini troughs north of Nordaustlandet, Svalbard – The importance of structural-geological setting in trough-mouth fan development. *Marine Geology*. https://doi.org/10.1016/j.margeo.2017.10.008

Frederick, B. C., Young, D. A., Blankenship, D. D., Richter, T. G., Kempf, S. D., Ferraccioli, F., & Siegert, M. J. (2016). Distribution of subglacial sediments across the Wilkes Subglacial Basin, East Antarctica. *Journal of Geophysical Research: Earth Surface*, *121*(4), 790–813. https://doi.org/10.1002/2015JF003760

Gales, J. A. (2013). *The geomorphology of Antarctic submarine slopes* (PhD Thesis). The University of Manchester.

Gales, J. A., Larter, R. D., Mitchell, N. C., & Dowdeswell, J. A. (2013). Geomorphic signature of Antarctic submarine gullies: Implications for continental slope processes. *Marine Geology*, *337*, 112–124.

Gales, J. A., Larter, R. D., Leat, P. T., & Jokat, W. (2016). Components of an Antarctic trough-mouth fan: examples from the Crary Fan, Weddell Sea. In Julian A Dowdeswell, M. Canals, M. Jakobsson, B. J. Todd, E. K. Dowdeswell, & K. A. Hogan (Eds.), *Atlas of Submarine Glacial Landforms: Modern, Quaternary and Ancient* (Vol. 46, pp. 377–378). Geological Society, London, Memoirs.

Gasson, E. G. W., DeConto, R. M., Pollard, D., & Clark, C. D. (2018). Numerical simulations of a kilometre-thick Arctic ice shelf consistent with ice grounding observations. *Nature Communications*, (1), 1510.

Gulick, S. P. S., Shevenell, A. E., Montelli, A., Fernandez, R., Smith, C., Warny, S., et al. (2017). Initiation and long-term instability of the East Antarctic Ice Sheet. *Nature*, *552*, 225–229.

Halberstadt, A. R. W., Simkins, L. M., Greenwood, S. L., & Anderson, J. B. (2016). Past ice-sheet behaviour: retreat scenarios and changing controls in the Ross Sea, Antarctica. *The Cryosphere*, *10*(3), 1003–1020. https://doi.org/10.5194/tc-10-1003-2016

Hall, J. K. (1990). Chukchi Borderland. In A. Grantz, L. Johnson, & J. F. Sweeney (Eds.), *The Arctic Ocean Region* (Vol. L, pp. 337–350). The Geological Society of America.

Hegewald, A. (2012). *The Chukchi Region-Arctic Ocean-Tectonic and Sedimentary Evolution* (PhD Thesis). Chemistry and Geoscience University of Jena.

Hegewald, A., & Jokat, W. (2013). Tectonic and sedimentary structures in the northern Chukchi region, Arctic Ocean. *Journal of Geophysical Research: Solid Earth*, *118*(7), 3285–3296. http://dx.doi.org/10.1002/jgrb.50282

Hill, J. C., & Driscoll, N. W. (2008). Paleodrainage on the Chukchi shelf reveals sea level history and meltwater discharge. *Marine Geology*, *254*(3), 129–151. https://doi.org/10.1016/j.margeo.2008.05.018

Hill, J. C., Driscoll, N. W., Brigham-Grette, J., Donnelly, J. P., Gayes, P. T., & Keigwin, L. (2007). New evidence for high discharge to the Chukchi shelf since the Last Glacial Maximum. *Quaternary Research*, *68*(2), 271–279.

Himmler, T., Sahy, D., Martma, T., Bohrmann, G., Plaza-Faverola, A., Bünz, S., et al. (2019). A 160,000-year-old history of tectonically controlled methane seepage in the Arctic. *Science Advances*, *5*(8). https://doi.org/10.1126/sciadv.aaw1450

Howat, I. M., Joughin, I., & Scambos, T. A. (2007). Rapid Changes in Ice Discharge from Greenland Outlet Glaciers. *Science*, *315*(5818), 1559–1561. https://doi.org/10.1126/science.1138478

Huang, Z., Siwabessy, J., Cheng, H., & Nichol, S. (2018). Using Multibeam Backscatter Data to Investigate Sediment-Acoustic Relationships. *Journal of Geophysical Research: Oceans*, *123*(7), 4649–4665. https://doi.org/10.1029/2017JC013638

Hughes, T., Denton, G., & Grosswald, M. (1977). Was there a late-Würm Arctic ice sheet? *Nature*, *266*(5603), 5967602.

Hunkins, K., Herron, T., Kutschale, H., & Peter, G. (1962). Geophysical studies of the Chukchi Cap, Arctic Ocean. *Journal of Geophysical Research*, *67*, 235–247.

Ilhan, I., & Coakley, B. J. (2018). Meso-Cenozoic evolution of the southwestern Chukchi Borderland, Arctic Ocean. *Marine and Petroleum Geology*, *95*, 100–109. https://doi.org/10.1016/j.marpetgeo.2018.04.014

Ivanov, V. V., Shapiro, G. I., Huthnance, J. M., Aleynik, D. L., & Golovin, P. N. (2004). Cascades of dense water around the world ocean. *Progress in Oceanography*, *60*(1), 47–98. https://doi.org/10.1016/j.pocean.2003.12.002

Jakobsson, M. (1999). First high-resolution chirp sonar profiles from the central Arctic Ocean reveal erosion of Lomonosov Ridge sediments. *Marine Geology*, *158*(1), 111–123. https://doi.org/10.1016/S0025-3227(98)00186-8

Jakobsson, M., Løvlie, R., Arnold, E. M., Backman, J., Polyak, L., Knutsen, J.-O., & Musatov, E. (2001). Pleistocene stratigraphy and paleoenvironmental variation from Lomonosov Ridge sediments, central Arctic Ocean. *Global and Planetary Change*, *31*(1), 1–22. https://doi.org/10.1016/S0921-8181(01)00110-2

Jakobsson, M., Gardner, J. V., Vogt, P. R., Mayer, L. A., Armstrong, A., Backman, J., et al. (2005). Multibeam bathymetric and sediment profiler evidence for ice grounding on the Chukchi Borderland, Arctic Ocean. *Quaternary Research*, *63*(2), 150–160. https://doi.org/10.1016/j.yqres.2004.12.004

Jakobsson, M., Polyak, L., Edwards, M., Kleman, J., & Coakley, B. J. (2008). Glacial geomorphology of the Central Arctic Ocean: the Chukchi Borderland and the Lomonosov Ridge. *Earth Surface Processes and Landforms*, *33*(4), 526–545. https://doi.org/10.1002/esp.1667

Jakobsson, M., Nilsson, J., O'Regan, M., Backman, J., Löwemark, L., Dowdeswell, J. A., et al. (2010). An Arctic Ocean ice shelf during MIS 6 constrained by new geophysical and geological data. *Quaternary Science Reviews*, *29*(25), 3505–3517. https://doi.org/10.1016/j.quascirev.2010.03.015

Jakobsson, M., Andreassen, K., Bjarnadóttir, L. R., Dove, D., Dowdeswell, J. A., England, J. H., et al. (2014). Arctic Ocean glacial history. *Quaternary Science Reviews*, *92*, 40–67. http://dx.doi.org/10.1016/j.quascirev.2013.07.033

Jakobsson, M., Nilsson, J., Anderson, L., Backman, J., Björk, G., Cronin, T. M., et al. (2016). Evidence for an ice shelf covering the central Arctic Ocean during the penultimate glaciation. *Nature Communications*, *7*.

Jakobsson, M., Mayer, L. A., Bringensparr, C., Castro, C. F., Mohammad, R., Johnson, P., et al. (2020). The International Bathymetric Chart of the Arctic Ocean Version 4.0. *Scientific Data*, (1), 176.

Joe, Y. J., Polyak, L., Schreck, M., Niessen, F., Yoon, S. H., Kong, G. S., & Nam, S.-I. (2020). Late Quaternary depositional and glacial history of the Arliss Plateau off the East Siberian margin in the western Arctic Ocean. *Quaternary Science Reviews*, *228*, 106099. https://doi.org/10.1016/j.quascirev.2019.106099

Jokat, W. (2009). *The Expedition of the Research Vessel "Polarstern" to the Arctic in 2008 (ARK-XXIII/3)*. Alfred Wegener Institute.

Kim, J.-H., Hachikubo, A., Kida, M., Minami, H., Lee, D.-H., Jin, Y. K., et al. (2020). Upwarding gas source and postgenetic processes in the shallow sediments from the ARAON Mounds, Chukchi Sea. *Journal of Natural Gas Science and Engineering*, *76*, 103223.

Kirkbride, M. P. (2002). 6 - Processes of glacial transportation. In J. Menzies (Ed.), *Modern and Past Glacial Environments* (pp. 147–169). Oxford: Butterworth-Heinemann. https://doi.org/10.1016/B978-075064226-2/50009-X

Klages, J. P., Kuhn, G., Graham, A. G. C., Hillenbrand, C.-D., Smith, J. A., Nitsche, F. O., et al. (2015). Palaeo-ice stream pathways and retreat style in the easternmost Amundsen Sea Embayment, West Antarctica, revealed by combined multibeam bathymetric and seismic data. *Geomorphology*, *245*, 207--222.

Laberg, J. S., Vorren, T. O., Dowdeswell, J. A., Kenyon, N. H., & Taylor, J. (2000). The Andøya Slide and the Andøya Canyon, north-eastern Norwegian–Greenland Sea. *Marine Geology*, *162*(2–4), 259–275. http://dx.doi.org/10.1016/S0025-3227(99)00087-0

Lisiecki, L. E., & Raymo, M. E. (2005). A Pliocene-Pleistocene stack of 57 globally distributed benthic delta18O records. *Paleoceanography*, *20*(1).

Lowe, A. L., & Anderson, J. B. (2002). Reconstruction of the West Antarctic ice sheet in Pine Island Bay during the Last Glacial Maximum and its subsequent retreat history. *Quaternary Science Reviews*, *21*(16–17), 1879–1897. http://dx.doi.org/10.1016/S0277-3791(02)00006-9

Lowe, A. L., & Anderson, J. B. (2003). Evidence for abundant subglacial meltwater beneath the paleo-ice sheet in Pine Island Bay, Antarctica. *Journal of Glaciology*, *49*(164), 125–138.

MacGregor, J. A., Fahnestock, M. A., Catania, G. A., Aschwanden, A., Clow, G. D., Colgan, W. T., et al. (2016). A synthesis of the basal thermal state of the Greenland Ice Sheet. *Journal of Geophysical Research: Earth Surface*, *121*(7), 1328–1350. https://doi.org/10.1002/2015JF003803

Matthiessen, J., Niessen, F., Stein, R., & Naafs, B. D. A. (2010). Pleistocene glacial marine sedimentary environments at the eastern Mendeleev Ridge, Arctic Ocean. *Polarforschung*, *79*(2), 123–137.

Menzies, J., & van der Meer, J. J. M. (2018). *Past Glacial Environments*. (J. Menzies & J. J. M. van der Meer, Eds.) (Second). Elsevier.

Menzies, J., & Shilts, B. W. (2002). 8 - Subglacial environments. In J. Menzies (Ed.), *Modern and Past Glacial Environments* (pp. 183–278). Oxford: Butterworth-Heinemann. https://doi.org/10.1016/B978-075064226-2/50011-8

Miramontes, E., Cattaneo, A., Jouet, G., Théreau, E., Thomas, Y., Rovere, M., et al. (2016). The Pianosa Contourite Depositional System (Northern Tyrrhenian Sea): Drift morphology and Plio-Quaternary stratigraphic evolution. *Marine Geology*, *378*, 20–42. https://doi.org/10.1016/j.margeo.2015.11.004

Moore, D. G. (1964). Shear strength and related properties of sediments from experimental mohole (Guadalupe site). *Journal of Geophysical Research (1896-1977)*, *69*(20), 4271–4291.

Niessen, F., Hong, J. K., Hegewald, A., Matthiessen, J., Stein, R., Kim, H., et al. (2013). Repeated Pleistocene glaciation of the East Siberian continental margin. *Nature Geosci*, *6*(10), 842–846. http://dx.doi.org/10.1038/ngeo1904

Noormets, R., Dowdeswell, J. A., Larter, R. D., Cofaigh, C. Ó., & Evans, J. (2009). Morphology of the upper continental slope in the Bellingshausen and Amundsen Seas – Implications for sedimentary processes at the shelf edge of West Antarctica. *Marine Geology*, *258*(1), 100–114. https://doi.org/10.1016/j.margeo.2008.11.011

Ó Cofaigh, C., Taylor, J., Dowdeswell, J. A., & Pudsey, C. J. (2003). Palaeo-ice streams, trough mouth fans and high-latitude continental slope sedimentation. *Boreas*, *32*(1), 37–55.

Ó Cofaigh, C., Dowdeswell, J. A., Evans, J., Kenyon, N. H., Taylor, J., Mienert, J., & Wilken, M. (2004). Timing and significance of glacially influenced mass-wasting in the submarine channels of the Greenland Basin. *Marine Geology*, *207*(1), 39–54. https://doi.org/10.1016/j.margeo.2004.02.009

Ó Cofaigh, C., Dowdeswell, J. A., Allen, C. S., Hiemstra, J. F., Pudsey, C. J., Evans, J., & Evans, D. [J A. (2005). Flow dynamics and till genesis associated with a marine-based Antarctic palaeo-ice stream. *Quaternary Science Reviews*, *24*(5), 709–740. https://doi.org/10.1016/j.quascirev.2004.10.006

Ó Cofaigh, C., Hogan, K. A., Dowdeswell, J. A., & Streuff, K. (2016). Stratified glacimarine basin-fills in West Greenland fjords. In J. A. Dowdeswell, M. Canals, M. Jakobsson, B. J. Todd, E. K. Dowdeswell, & K. A. Hogan (Eds.), *Atlas of Submarine Glacial Landforms: Modern, Quaternary and Ancient* (Vol. 46, pp. 99–100). Geological Society, London, Memoirs.

Ó Cofaigh, C., Hogan, K. A., Jennings, A. E., Callard, S. L., Dowdeswell, J. A., Noormets, R., & Evans, J. (2018). The role of meltwater in high-latitude trough-mouth fan development: The Disko Trough-Mouth Fan, West Greenland. *Marine Geology*, *402*, 17–32. https://doi.org/10.1016/j.margeo.2018.02.001

O'Grady, D. B., & Syvitski, J. P. (2002). Large-scale morphology of Arctic continental slopes: the influence of sediment delivery on slope form. In Julian A Dowdeswell & C. Ó Cofaigh (Eds.), *SPECIAL PUBLICATION-GEOLOGICAL SOCIETY OF LONDON* (Vol. 203, pp. 11–32). The Geological Society of London.

O'Regan, M., Backman, J., Barrientos, N., Cronin, T. M., Gemery, L., Kirchner, N., et al. (2017). The De Long Trough: a newly discovered glacial trough on the East Siberian continental margin. *Climate of the Past*, *13*(9), 1269–1284. https://doi.org/10.5194/cp-13-1269-2017

Ottesen, D., & Dowdeswell, J. A. (2006). Assemblages of submarine landforms produced by tidewater glaciers in Svalbard. *Journal of Geophysical Research: Earth Surface*, *111*(F1). Retrieved from https://agupubs.onlinelibrary.wiley.com/doi/abs/10.1029/2005JF000330

Ottesen, D., & Dowdeswell, J. A. (2009). An inter–ice-stream glaciated margin: Submarine landforms and a geomorphic model based on marine-geophysical data from Svalbard. *Geological Society of America Bulletin*, *121*(11–12), 1647–1665.

Ottesen, D., Rise, L., Knies, J., Olsen, L., & Henriksen, S. (2005). The Vestfjorden-Trænadjupet palaeo-ice stream drainage system, mid-Norwegian continental shelf. *Marine Geology*, *218*(1), 175–189. https://doi.org/10.1016/j.margeo.2005.03.001

Piper, D. J. W., & Normark, W. R. (2009). Processes That Initiate Turbidity Currents and Their Influence on Turbidites: A Marine Geology Perspective. *Journal of Sedimentary Research*, *79*(6), 347–362. https://doi.org/10.2110/jsr.2009.046

Piper, D. J. W., Deptuck, M., Mosher, D., Hughes Clarke, J., & Migeon, S. (2012). *Erosional and depositional features of glacial meltwater discharges on the eastern Canadian continental margin*. (B. Prather, M. E. Deptuck, D. Mohrig, B. van Hoorn, & R. Wynn, Eds.), *Applications of the Principles of Seismic Geomorphology to Continental Slope and Base-of-slope Systems: Case Studies from Seafloor and Near-Seafloor Analogues. Edited by BE Prather, ME Deptuck, D. Mohrig, B. van Hoorn, and R. Wynn. Society for Sedimentary Geology (SEPM), Special Publications* (Vol. 99, p. 80). SEPM.

Polyak, L., Forman, S. L., Herlihy, F. A., Ivanov, G., & Krinitsky, P. (1997). Late Weichselian deglacial history of the Svyataya (Saint) Anna Trough, northern Kara Sea, Arctic Russia. *Marine Geology*, *143*(1), 169–188. https://doi.org/10.1016/S0025-3227(97)00096-0

Polyak, L., Edwards, M. H., Coakley, B. J., & Jakobsson, M. (2001). Ice shelves in the Pleistocene Arctic Ocean inferred from glaciogenic deep-sea bedforms. *Nature*, *410*, 453–457.

Polyak, L., Darby, D. A., Bischof, J. F., & Jakobsson, M. (2007). Stratigraphic constraints on late Pleistocene glacial erosion and deglaciation of the Chukchi margin, Arctic Ocean. *Quaternary Research*, *67*(2), 234–245. https://doi.org/10.1016/j.yqres.2006.08.001

Polyak, L., Best, K. M., Crawford, K. A., Council, E. A., & St-Onge, G. (2013). Quaternary history of sea ice in the western Arctic Ocean based on foraminifera. *Quaternary Science Reviews*, *79*, 145–156. https://doi.org/10.1016/j.quascirev.2012.12.018

Pope, E. L., Talling, P. J., & Ó Cofaigh, C. (2018). The relationship between ice sheets and submarine mass movements in the Nordic Seas during the Quaternary. *Earth-Science Reviews*, *178*, 208–256. https://doi.org/10.1016/j.earscirev.2018.01.007

Rebesco, M., & Camerlenghi, A. (2008). Late Pliocene margin development and mega debris flow deposits on the Antarctic continental margins: Evidence of the onset of the modern Antarctic Ice Sheet? *Palaeogeography, Palaeoclimatology, Palaeoecology*, *260*(1), 149–167. https://doi.org/10.1016/j.palaeo.2007.08.009

Rebesco, M., Özmaral, A., Urgeles, R., Accettella, D., Lucchi, R. G., Rüther, D., et al. (2016). Evolution of a high-latitude sediment drift inside a glacially-carved trough based on high-resolution seismic stratigraphy (Kveithola, NW Barents Sea). *Quaternary Science Reviews*, *147*(Special Issue: PAST Gateways (Palaeo-Arctic Spatial and Temporal Gateways)), 178–193. http://dx.doi.org/10.1016/j.quascirev.2016.02.007

Rydningen, T. A., Laberg, J. S., & Kolstad, V. (2015). Seabed morphology and sedimentary processes on high-gradient trough mouth fans offshore Troms, northern Norway. *Geomorphology*, *246*, 205–219. http://dx.doi.org/10.1016/j.geomorph.2015.06.007

Schomacker, A., Kjær, K. H., & Krüger, J. (2010). 8 Subglacial Environments, Sediments and Landforms at the Margins of Mýrdalsjökull. In A. Schomacker, J. Krüger, & K. H. Kjær (Eds.), *The Mýrdalsjökull Ice Cap, Iceland. Glacial processes, sediments and landforms on an active volcano* (Vol. 13, pp. 127–144). Elsevier. https://doi.org/10.1016/S1571-0866(09)01308-6

Schreck, M., Nam, S.-I., Polyak, L., Vogt, C., Kong, G.-S., Stein, R., et al. (2018). Improved Pleistocene sediment stratigraphy and paleoenvironmental implications for the western Arctic Ocean off the East Siberian and Chukchi margins. *Arktos*, *4*(1), 21. https://doi.org/10.1007/s41063-018-0057-8

Shaver, R., & Hunkins, K. (1964). Arctic ocean geophysical studies: Chukchi Cap and Chukchi abyssal plain. *Deep Sea Research and Oceanographic Abstracts*, *11*(6), 905–916. https://doi.org/10.1016/0011-7471(64)90340-7

Shipp, S. S., Anderson, J., & Domack, E. (1999). Late Pleistocene–Holocene retreat of the West Antarctic Ice-Sheet system in the Ross Sea: part 1—geophysical results. *Geological Society of America Bulletin*, *111*(10), 1486–1516.

Solheim, A., Faleide, J. I., Andersen, E. S., Elverhøi, A., Forsberg, C. F., Vanneste, K., et al. (1998). Late Cenozoic Seismic Stratigraphy And Glacial Geological Development Of The East Greenland And Svalbard--Barents Sea Continental Margins. *Quaternary Science Reviews*, *17*(1), 155–184. https://doi.org/10.1016/S0277-3791(97)00068-1

Stein, R., Matthießen, J., Niessen, F., Krylov, A., Nam, S., & Bazhenova, E. (2010). Towards a better (litho-) stratigraphy and reconstruction of Quaternary paleoenvironment in the Amerasian Basin (Arctic Ocean). *Polarforschung*, *79*(2), 97–121.

Stewart, M. A., & Lonergan, L. (2011). Seven glacial cycles in the middle-late Pleistocene of northwest Europe: Geomorphic evidence from buried tunnel valleys. *Geology*, *39*(3), 283–286. https://doi.org/10.1130/G31631.1

SWERUS Scientific Party. (2016). *Cruise Report SWERUS-C3 Leg 2*.

Taylor, J., Dowdeswell, J. A., Kenyon, N. H., & Ó Cofaigh, C. (2002). Late Quaternary architecture of trough-mouth fans: debris flows and suspended sediments on the Norwegian margin. In Julian A Dowdeswell & C. Ó Cofaigh (Eds.), *Glacier-influenced sedimentation on high-latitude continental margins* (pp. 55–71). The Geological Society of London. https://doi.org/10.1144/GSL.SP.2002.203.01.04

Todd, B. J., Valentine, P. C., Longva, O., & Shaw, J. (2007). Glacial landforms on German Bank, Scotian Shelf: evidence for Late Wisconsinan ice-sheet dynamics and implications for the formation of De Geer moraines. *Boreas*, *36*(2), 148–169. https://doi.org/10.1111/j.1502-3885.2007.tb01189.x

Veeken, P. C. H., & van Moerkerken, B. (2013). *Seismic Stratigraphy and Depositional Facies Models*. EAGE publications.

Vorren, T. O., & Laberg, J. S. (1997). Trough mouth fans—palaeoclimate and ice-sheet monitors. *Quaternary Science Reviews*, *16*(8), 865–881.

Wang, R., Xiao, W., März, C., & Li, Q. (2013). Late Quaternary paleoenvironmental changes revealed by multi-proxy records from the Chukchi Abyssal Plain, western Arctic Ocean. *Global and Planetary Change*, *108*, 100–118. https://doi.org/10.1016/j.gloplacha.2013.05.017

Wellner, J. S., Lowe, A. L., Shipp, S. S., & Anderson, J. B. (2001). Distribution of glacial geomorphic features on the Antarctic continental shelf and correlation with substrate: implications for ice behavior. *Journal of Glaciology*, *47*(158), 397–411. https://doi.org/10.3189/172756501781832043

Wellner, J. S., Heroy, D. C., & Anderson, J. B. (2006). The death mask of the antarctic ice sheet: Comparison of glacial geomorphic features across the continental shelf. *Geomorphology*, *75*(1), 157–171. https://doi.org/10.1016/j.geomorph.2005.05.015

Wille, P. (2005). *Sound images of the ocean: in research and monitoring* (Vol. 1). Springer Science & Business Media.

Winsborrow, M. C. M., Clark, C. D., & Stokes, C. R. (2010). What controls the location of ice streams? *Earth-Science Reviews*, *103*(1–2), 45–59. http://dx.doi.org/10.1016/j.earscirev.2010.07.003

Zaragosi, S., Auffret, G. A., Faugères, J.-C., Garlan, T., Pujol, C., & Cortijo, E. (2000). Physiography and recent sediment distribution of the Celtic Deep-Sea Fan, Bay of Biscay. *Marine Geology*, *169*(1), 207–237.